AD-A077 295 BOSTON COLL CHESTNUT HILL MASS SPACE DATA ANALYSIS LAB F/G 4/1
ANALYSIS OF AURORAL ELECTRON DATA.(U)
MAY 78 E R HEGBLOM F19628-74-C-0176
UNCLASSIFIED BC-SDAL-77-3 AFGL-TR-78-0127 NL

1 OF 1
AD-
A077295

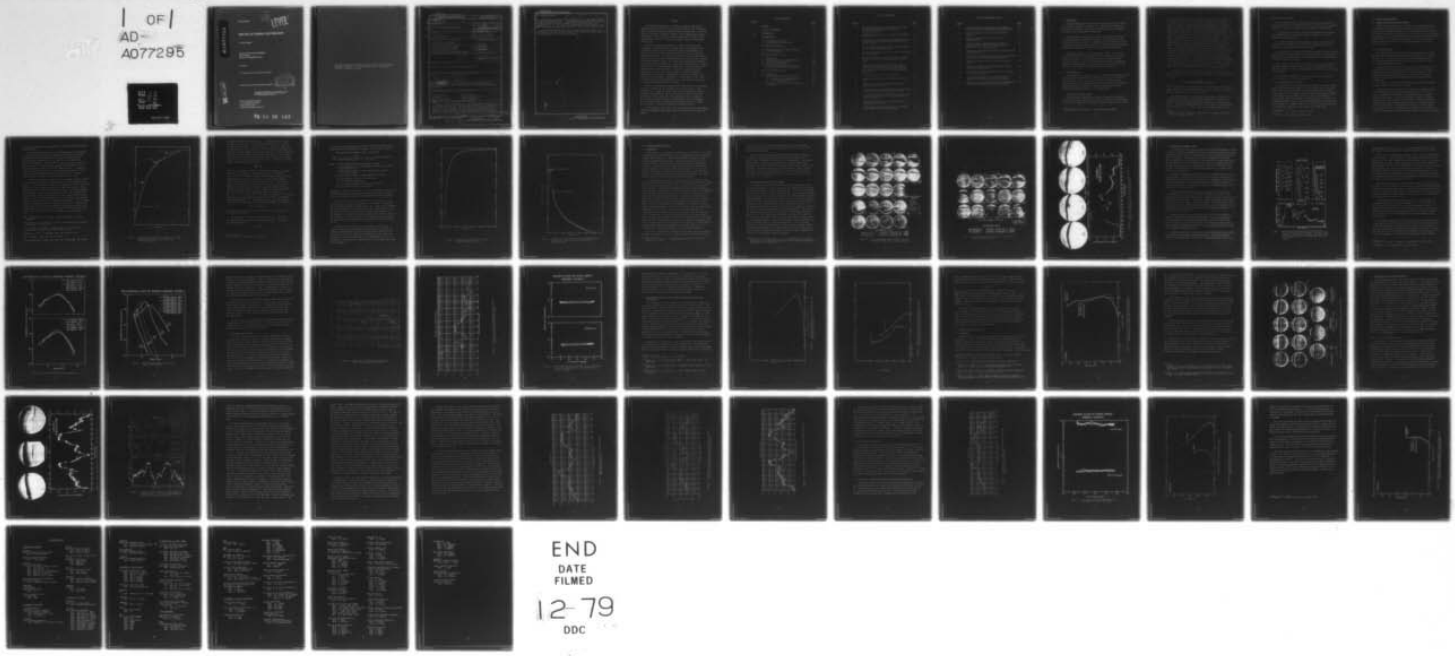

END
DATE
FILMED
12-79
DDC

AFGL-TR-79-0127

LEVEL II

ANALYSIS OF AURORAL ELECTRON DATA

E. Richard Hegblom

SPACE DATA ANALYSIS LABORATORY
Boston College
Chestnut Hill, Massachusetts 02167

1 May 1978

Final Report for period 1 June 1974 - 31 May 1977

Approved for public release; distribution unlimited

This research was sponsored by the Defense Nuclear Agency under Subtask L25AAXHX632, Work Unit 64, entitled IP Phenomenology/Optical Experiment.

Air Force Geophysics Laboratory
Air Force Systems Command
United States Air Force
Hanscom AFB, Massachusetts 01731

Qualified requestors may obtain additional copies from the Defense Documentation Center. All others should apply to the National Technical Information Service.

UNCLASSIFIED

SECURITY CLASSIFICATION OF THIS PAGE (When Data Entered)

REPORT DOCUMENTATION PAGE	READ INSTRUCTIONS BEFORE COMPLETING FORM
1. REPORT NUMBER: AFGL-TR-78-0127	2. GOVT ACCESSION NO. / 3. RECIPIENT'S CATALOG NUMBER
4. TITLE (and Subtitle): ANALYSIS OF AURORAL ELECTRON DATA.	5. TYPE OF REPORT & PERIOD COVERED: Final Report, 1 June 1974 — 31 May 1977
	6. PERFORMING ORG. REPORT NUMBER: BC-SDAL-77-3
7. AUTHOR(s): E. Richard Hegblom	8. CONTRACT OR GRANT NUMBER(s): F19628-74-C-0176
9. PERFORMING ORGANIZATION NAME AND ADDRESS: Trustees of Boston College, Chestnut Hill, Massachusetts 02167	10. PROGRAM ELEMENT, PROJECT, TASK AREA & WORK UNIT NUMBERS: CDNA24AF; 62304H; 62710H
11. CONTROLLING OFFICE NAME AND ADDRESS: Air Force Geophysics Laboratory, Hanscom AFB, Massachusetts 01731, Contract Monitor: Mr. John Sandock (OPR)	12. REPORT DATE: 1 May 1978
	13. NUMBER OF PAGES: 57
14. MONITORING AGENCY NAME & ADDRESS (if different from Controlling Office)	15. SECURITY CLASS. (of this report): Unclassified
	15a. DECLASSIFICATION/DOWNGRADING SCHEDULE

16. DISTRIBUTION STATEMENT (of this Report)

Approved for public release; distribution unlimited

17. DISTRIBUTION STATEMENT (of the abstract entered in Block 20, if different from Report)

CDNA, 24, X632

18. SUPPLEMENTARY NOTES

This research was sponsored by the Defense Nuclear Agency under Subtask L25AAXHX632, Work Unit 64, entitled IP Phenomenology/Optical Experiment.

19. KEY WORDS (Continue on reverse side if necessary and identify by block number)

Auroral Electrons	Project ICECAP
Energy Spectra	Particle Precipitation
Electrostatic Analyzer	Energy Deposition

20. ABSTRACT (Continue on reverse side if necessary and identify by block number)

Auroral electron data obtained by rocket measurements as part of the ICECAP program are analyzed. The measurements were made by a spherical plate electrostatic analyzer along with scintillators. The differential energy spectra of electrons measured in each of the rocket flights were quite different. In one flight the spectra (measured from 4 to 30 keV) peaked at 16 keV (full width half maximum ~8 keV) as the rocket overflew the auroral about

(Cont.)

DD FORM 1 JAN 73 1473 EDITION OF 1 NOV 65 IS OBSOLETE

UNCLASSIFIED

SECURITY CLASSIFICATION OF THIS PAGE (When Data Entered)

20. Abstract (Cont.)

arc (maximum energy deposition ~30 ergs/cm^2-sec-sr). As the rocket overflew the arc in the second flight, peak appeared in the spectra near 12 keV and shifted to beyond 30 keV in the region of maximum precipitation (>100 ergs/cm^2-sec-sr). In this region the measured spectra were relatively flat with the differential intensity a factor of 3 higher at 30 keV than at 4 keV.

The ion-electron production rate is calculated for each flight. The 3914Å emission rate and the electron density are computed from the production rate and compared with the rocket measurements.

PREFACE

The Defense Nuclear Agency is conducting a High Altitude Effects Simulation Program (HAES) in order to provide information for the development and testing of predictive computer codes which are used to assess the operation of various Department of Defense radar, communications, optical and infrared systems in nuclear disturbed environments. Under the HAES program there are various interrelated programs including field measurement programs.

One of these measurement programs is ICECAP (Infrared Chemistry Experiments - Coordinated Auroral Program) which is a coordinated field measurement program to study ionization and excitation mechanisms and chemical processes producing infrared emissions in the upper atmosphere during auroral events. This report discusses the results of data obtained during the flights of multi-instrumented rockets into aurora from the Poker Flat Research Range in Alaska. The rocket payloads contained instruments to measure precipitating particles, visible and infrared emissions, electron and ion density, and ion and neutral composition. In addition there were numerous ground based instruments including the Chatanika Incoherent Scatter Radar, all-sky and television cameras, scanning photometers, radiometers, interferometers, magnetometers, ionosondes, riometers and a partial reflection sounder. The emphasis in this report will be on the precipitating particle measurements made by an electrostatic analyzer and a scintillator detector flown on the rockets.

We wish to acknowledge and thank various particicipants in the program for their assistance and for valuable discussions of the data. These include Dr. A. T. Stair, Mr. James Ulwick, Mr. John Sandock, Mr. Phillip Doyle, Mr. Robert McInerney and Mr. John Kotelly of AFGL; Mr. William Grieder, Mr. Dennis Delorey, Mr. Paul Pruneau, Mr. Brian Sullivan and Mr. Leo Power of Boston College; Dr. William Reidy and Mr. Orr Shepherd, Mr. Albert Hurd and Mr. William Sheehan of Visidyne; and Dr. Kay Baker, Mr. Carl Howlett and Mr. David Burt of Utah State University.

A special thanks to Mrs. Carol Foley of Boston College for her computer system and programming contributions and to Ms. Mary Kelly for typing this report.

TABLE OF CONTENTS

LIST OF ILLUSTRATIONS

LIST OF ILLUSTRATIONS (Cont.)

1.0 INTRODUCTION

This final report covers the analysis of data taken by rocket flights into disturbed ionospheric conditions (e.g., auroras) and includes the calculation of production rates, optical emission rates and a comparison of rocket-borne and ground-based observations.

The measurements discussed here include the energetic electron precipitation measured by electrostatic analyzers, and scintillators flown on rockets into visible auroras. Calculations of the production rate, the volume emission rate of various transitions as well as the electron density are made and compared with rocketborne and ground-based measurements.

The data were taken as part of DNA Project ICECAP*. The objective of the ICECAP program is to investigate the various mechanisms for the production of short (1-6 μm) and long (6-30 μm) wavelength infrared emissions in aurora. As part of this program various multi-instrumented rockets have been launched into aurora to measure the energy input, the ionization, and the optical and infrared emissions produced.

2.0 INSTRUMENTATION

The instruments for particle detection include an electrostatic analyzer (ESA) to measure the differential intensity of electrons with energies from about 3 to 30 keV, a scintillator detector to measure the total particle energy for electrons with energies greater than 4 keV and protons greater than 30 keV, and particle counters for measuring the flux of electrons with energies greater 17, 22, 42 and 88 keV.

2.1 Electrostatic Analyzer (ESA)

The electrostatic analyzer was designed to measure the differential intensity of electrons with energies from 3 to 30 keV with an energy resolution of 10%. The analyzer utilized two concentric plates that were in the

*Infrared Chemistry Experiments - Coordinated Auroral Program

shape of spherical octants, with a varying potential applied between them to transmit electrons of a specific energy, depending on the voltage between the plates. The outer plate was grounded and the inner plate had a positive potential applied to it, which was exponentially swept from about 3 keV to about 10 volts with a time constant of 90 milliseconds. The sweep was repeated every 0.5 seconds. This voltage was chopped with a 1 kHz square wave to modulate the current transmitted was through the analyzer plates. The transmitted electrons were detected by a CaF_2 (Eu) scintillator which was optically coupled to an EMR 541-D photomultiplier. A thin aluminum coating (~1000Å) was applied to the face of the scintillator to prevent stray light from reaching the photomultiplier. A potential of about 3 kV was applied to the coating to accelerate the transmitted electrons and thereby extend the response of the instrument to lower energy electrons. A temperature compensated logarithmic amplifier with a narrow bandpass filter, which was tuned to the 1 kHz plate modulation frequency, measured the photomultiplier current. The amplifier output was rectified, integrated (.01 second time constant) and telemetered to a ground station. The sweep, post accelerator and photomultiplier high voltages, and all low voltage power supplies and the temperature were monitored during the flights.

The differential intensity, $\frac{dJ}{dE}$ $(cm^2\text{-sec-sr-keV})^{-1}$ of electrons of energy E was calculated from the measured photomultiplier current I through the equation

$$\frac{dJ}{dE} = \frac{(I-I_n)}{(S)(KE)(A\Omega)(E+E_{pA}-E_L)(1-K_B R_B)}$$

where S is the ratio of the photomultiplier output current to the rate of energy deposition in the scintillator and I_n is the average noise determined from the current data at the end of the sweep.

The absolute value of S was obtained by measuring the response to a calibrated Am^{241} α-particle source and multiplying this by the ratio of electrons to alpha particle scintillation efficiency at a fixed electron energy. The electron energy dependence of S was calculated using the X-Ray data of Aitken[1] et. al. [1967]. This was subsequently checked with an

[1] Aitken, D. W., B. L. Beron, T. Yenicay and H. R. Zulliger, IEEE Trans. Nucl. Sci., NS-14, 468, 1967.

electron beam calibration.

K is the inherent energy resolution of the plates (4%) measured with an electron beam over the energy range from 2 to 15 keV and is in agreement within 20% of the value calculated from the dimensions of the plates.

$A\Omega$ is the geometric factor (.09 cm^2-sr) calculated from the area of the viewing aperture (3 cm^2) and the angular response (6 1/2° x 16°) measured with an electron beam.

K_b is the fractional mean energy of the electrons backscattered by the scintillator [Sternglass, 1954][(2)] and R_b is the fraction of the incident electrons backscattered [Palluel, 1947][(3)].

E_{pa} represents the energy acquired by the electrons due to the potential applied to the aluminum coating on the scintillator and E_L is the average energy lost per incident electron in the aluminum coating, calculated from the measured aluminum thickness.

This equation, (and effectively the values of S, E_L, R_b and K_b) has been checked after the flight with an electron beam measurement of the instrument response. There is good agreement (within 20% at 3 keV) between the two methods.

The instrument is mounted on the rocket so that the center of the field of view is at 45° to the rocket axis.

2.2 Energy Deposition Scintillator

The energy deposition scintillator which responds to the total energy deposited by electrons and protons over certain energy ranges consists of a thin (.035") scintillation phosor (plastic pilot B) which is viewed by a photomultiplier. The output is then amplified and telemetered to ground. A thin aluminum coating (1450Å) covers to surface of the phosphor to prevent ambient light from reaching the photomultiplier. This results in a minimum detectable energy of 4 keV for electrons and 30 keV for protons. The instrument has a geometric factor of 0.14 cm^2-sr (11° half-angle) and is located at any angle of 55° with respect to the rocket axis.

---

(2) Sternglass, E. J., Phys. Rev. 95, 345, 1954.

(3) Palluel, P., Compt. Rend., 224, 1492, 1947.

3.0 ELECTRON BEAM CALIBRATION

3.1 Energy Resolution and Angular Response

The ESAs were calibrated prior to flight in a vacuum chamber with an electron gun to determine the energy resolution of the plates (~4%), the overall energy resolution (determined by the integrating time of the amplifier and the time constant of the sweep, ~10%) and ratio of the plate voltage to beam energy (~10%). The angular response of the plates has been previously measured to be 16° x 6° with an electron beam. The area of the entrance aperture formed by the plates is 2.9 cm^2 and the geometric factor is 9.3×10^{-2} cm^2-sr.

3.2 Low Energy Response

The ESAs which were flown during the ICECAP program were recovered and subsequently calibrated with an electron beam primarily to accurately determine the low energy electron response. The instrument was placed in a vacuum chamber equipped with an electron gun and electrons from 0.5 to 6.0 keV were measured by the ESA.

The ESA plate voltage, the post accelerator high voltage and the photomultiplier high voltage were externally controlled. The photomultiplier anode current was measured with an external electrometer. The electrons passing through the plates were collected on the aluminum coating on the scintillator and transmitted by a shielded cable to an external meter.

The linearity of the photomultiplier at high currents was confirmed for anode currents less than about 10^{-5} amps.

A problem with this technique is the number of secondaries produced by the electron beam incident on the aluminum coating. If no bias voltage is applied to the coating, the secondaries produce a negative current to the coating. As the post accelerator voltage is increased, however, there is an increase in the collection of secondary electrons produced by the beam hitting the analyzer plates. This effect produces a current which must be subtracted from the measured current to obtain the true beam current. The measurements were made with 1, 2.45 and 2.8 kilovolts (flight post-accelerator voltages) applied to the post accelerator.

A 1 keV post accelerator voltage represents a resonable voltage to minimize these two effects.

The measurements were made for various beam energies and a normalized set of curves was plotted for each instrument of the ratio of the photomultiplier current to the product of the current from the aluminum coating and the total energy ($E + E_{pa}$), where E is the energy of the electrons transmitted by the plates and E_{pa} the energy acquired due to the post accelerator. For each value of E_{pa} (and each instrument) a set of curves was produced a sample of which is shown in Figure 1. A composite curve was constructed using the 1 keV post-accelerator curve up to 6 keV total energy and the higher energy portions of the curves for higher post-accelerator settings to extend the response curve to 9 keV.

In order to determine the response of the instrument at higher energies, the alpha particle calibration and the ratio of the α pulse height/β pulse height = 1/4[4],[5] was used. However, the response of the CaF_2 scintillator below 660 keV is non-linear and this must be taken into account in determining the response of the ESA between 9 and 30 keV. The energy dependence of the response of the CaF_2 scintillator to electrons was calculated using the X-ray data of Aitken et al [1967][6] with the energy of the electrons incident on the scintillator determined from the thickness of the aluminum coating (~1100Å) and the results of Kanter and Sternglass[7] for the average energy of an electron transmitted through an aluminum foil. The fraction of the energy dissipated in an aluminum foil is approximately (within ~20%) a linear function of the fraction of the range[8],[9], for electrons with energies from 2.5 to 40 keV. One can determine the fraction energy

---

(4) E. der Mateosian and M. Goldhaber, Brookhaven National Lab. Report (BNL 8417).

(5) J. Menefee, C. F. Swinehart, E. W. O'Dell, IEEE Transactions on Nuclear Science, NS-13, 720-724, 1966.

(6) D. W. Aitken, B. L. Beron, G. Yenican, and H. R. Zulliger, IEEE Transactions on Nuclear Science NS-14, 468-477, 1967.

(7) Kantor, H., and E. J. Sternglass, Phys. Rev. 126, 620 (1962).

(8) J. R. Young, J. Appl. Phys. 28, 524 (1957).

(9) W. Ehrenberg and J. Franks, Proc. Phys. Soc. (London) B66, 1057 (1953).

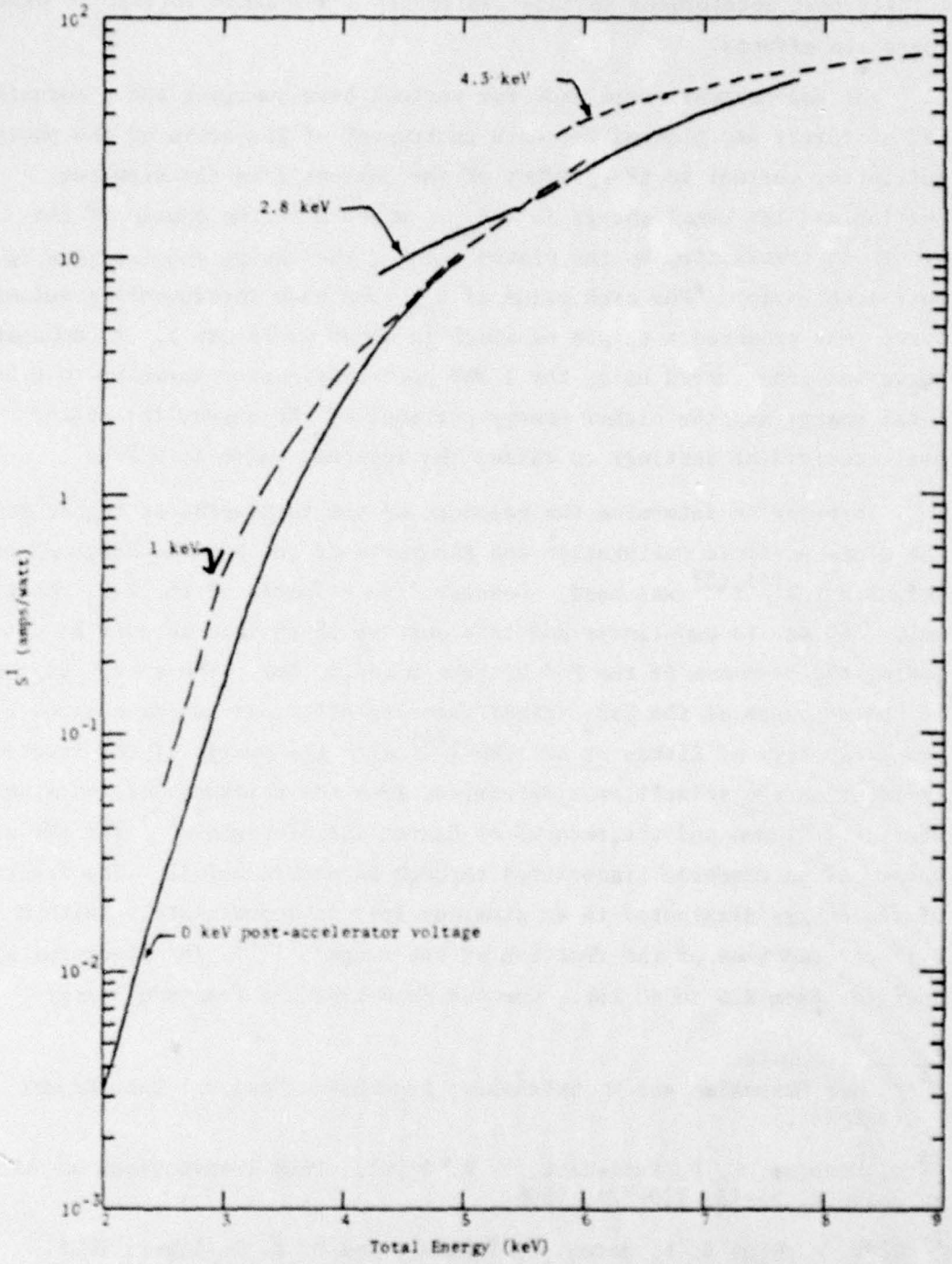

Figure 1. The response of the ESA as a function of the total incident electron energy for various post accelerator voltages.

transmitted through the aluminum foil as, $1 - \frac{\Delta W}{EI}$ where ΔW is the energy dissipated in the foil, E is the incident electron energy and I is the incident electron current. The sensitivity, S is then $K\xi_E(1 - \frac{\Delta W}{EI})$ where K is the response of the scintillator to 660 keV electrons, determined from the Am^{241} α-particle response and the ratio of electron to alpha scintillator efficiency for 5 MeV alphas and 660 keV electrons and ξ_E is the variation of this response at lower electron energies. The fraction of the energy dissipated in the foil (plus the dead layer of the scintillator) is approximately a linear fraction of the range

$$\frac{\Delta W}{EI} \approx \frac{\Delta X}{R}$$

where ΔX is the thickness of the foil plus the dead layer in the scintillator and R is the range of electrons with energy E. The equation $R = 11.5 \times 10^{-6} E^{1.35}$ where R is gm/cm^2 and E in keV is used for electrons with energies less than 10.5 keV and $R = 2.5 \times 10^{-6} E^2$ for electron energies greater than 10.5 keV and less than 30 keV[10]. The effective range ΔX, which includes the scintillator dead layer was determined by matching the measured sensitivity from 6 to 9 keV with the sensitivity determined from the equation $S = K\xi_E (1 - \frac{\Delta X}{R})$ with ΔX chosen to give the best fit to the data. The corresponding energy in the equation $\Delta X = 11.5 \times 10^{-6} E^{1.35}$ was 5.2 keV. This energy corresponds to the critical energy (which in turn corresponds to the practical range) E_c as defined by Kanter and Sternglass[7]. The threshold energy E_{th} is approximately $0.7\ E_c$ and the average energy of any penetrating electron E_a is given by[7]

$$E_a = 0.92(E_p - E_{th})$$

and this is used to determine the scintillator sensitivity function ξ_E as a function of energy.

The sensitivity S is then calculated from $S = K\xi_E(1 - \frac{\Delta X}{R})$ using the appropriate equation for R as a function of energy. A normalized sensitivity defined as

$$S = S/K$$

[10] J. R. Young, J. Appl. Phys. 27, 1 (1956).

was plotted for each instrument and since the agreement was within 20% a universal curve was used for each instrument. This is shown in Figure 2.

The data reduction equation using S then becomes

$$\frac{dJ}{dE} = \frac{(I-I_n)}{(.04E)(A\Omega)(K)(E+E_{PA})(S')\ 1.6 \cdot 10^{-19} \times 10^3} \ (cm^2\text{-sec-sr-keV})^{-1}$$

where I is the photomultiplier anode current in amperes

I_n is the average noise level determined when the plate voltage is approximately zero

E is the electron energy (in keV) transmitted by the plates ($\simeq$10 x plate voltage)

E_{PA} is the post accelerator voltage applied to the plates

$A\Omega$ is the geometric factor ($4.2 \times 10^{-2} cm^2\text{-sr}$)

K is 4 x α-particle sensitivity

S' is the normalized sensitivity plotted in figure 2.

.04E is the energy resolution of the plates

The geometric factor is reduced by 1/2 in later instruments due to a grid which was placed in front of the entrance aperture and kept at ground potential to reduce the effect of the ESA sweep on the rocket potential.

Figure 3 is a plot of the calibration for the ESA flown on rocket 18.219-1 in which the low energy response was calculated. The same ESA was refurbished and flown on Rocket IC519.07-1B. In this case an aluminum coating of approximatley the same thickness was reapplied to the face of the scintillator and the electron beam calibration was performed. For the purposes of comparison the actual calibration for the ESA on IC519.07-1B was divided by 2 in order to account for the effect of the screen which was used in front of the aperture on Rocket IC519.07-1B but not on Rocket 18.219-1.

In addition to the Am^{241} α-particle calibration a Fe^{55} X-ray source was also used. After taking into account the α/β ratio for the α-particle measurement[4] and the fluorescent response function[6] for $CaF_2(Eu)$, the ratio of the response (K) determined from the α-particle measurement to that calculated from the Fe^{55} measurement was 0.75. This discrepancy is apparently due to uncertainties in the various normalizing factors employed.

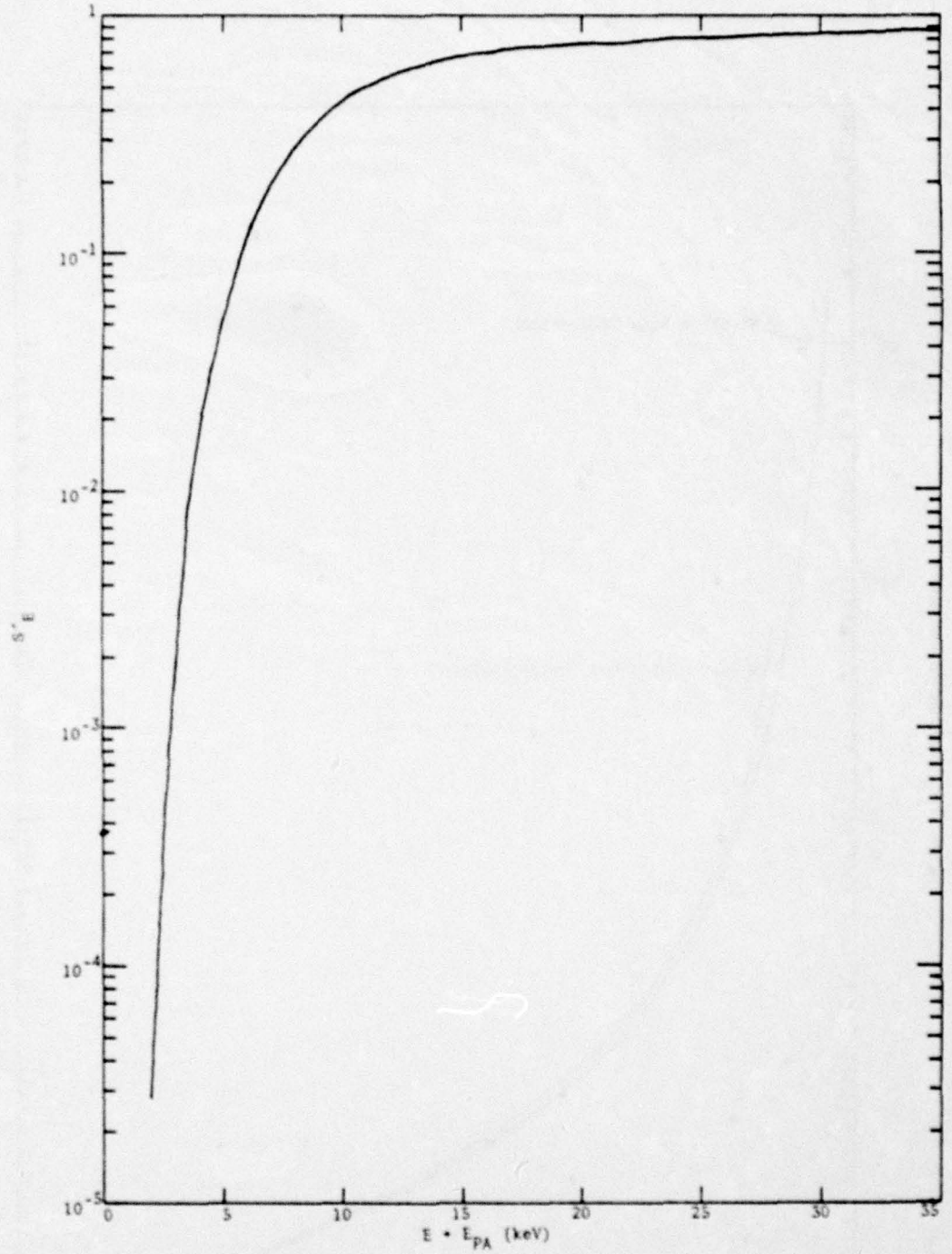

Figure 2. Normalized sensitivity (S′) vs. total electron energy for the ESA.

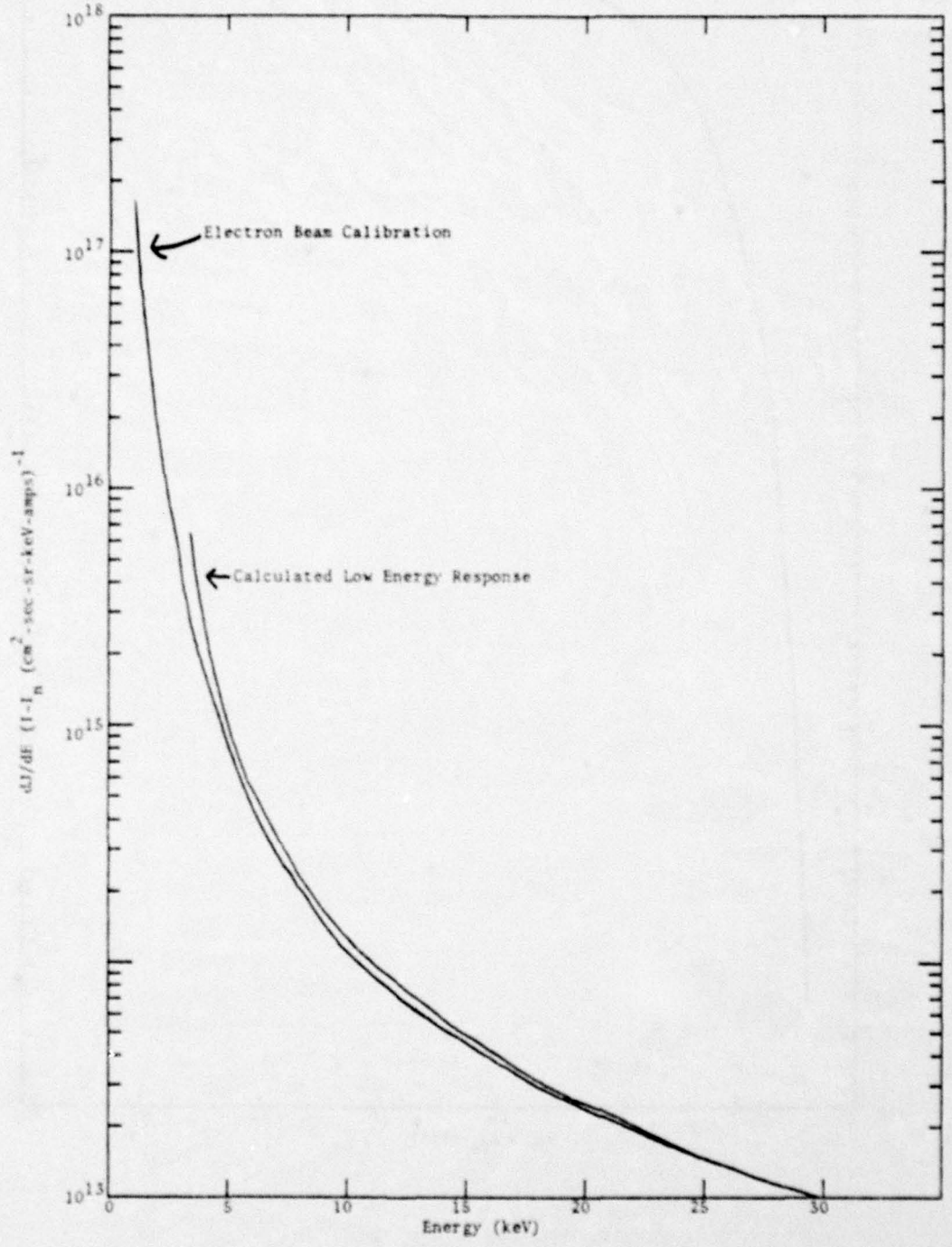

Figure 3. Comparison of calculated low energy response with the measured low energy response for the ESA flown on Rocket A18.219-1.

4.0 RESULTS FOR ROCKET A18.205-1

4.1 Introduction

Rocket A18.205-1 was launched on 27 March 1973 at 09:37:45 UT (~21:30 MLT) from the Poker Flat Research Range, Alaska, (geomagnetic latitude ~65°N) into a bright stable auroral arc. The rocket trajectory plane made an angle of 16° with the magnetic meridian plane. The rocket apogee was 181 km, the range was about 220 km and it had a horizontal velocity of approximately 0.6 km/sec. The rocket had an attitude control system which oriented the rocket to within 4° of the local vertical from 70 seconds to at least 375 seconds. The rocket axis made an angle with the magnetic field that varied from 9.5° to 13° during this period. At the end of the flight a parachute recovery system was operated and the payload was recovered.

The rocket payload included[11] instruments to measure electron fluxes, including the differential energy spectra, ion and neutral composition, electron and ion densities and temperature as well as infrared, visible, and ultraviolet emissions. Ground based measurements furnished by the University of Alaska included all-sky cameras, meridian scanning photometers, 3-axis magnetometers and 30 MHz riometers located at Poker Flat and Ft. Yukon and also all-sky cameras, meridian scanning photometers, an auroral television at Ester Dome, and an ionosonde at College, Alaska. The Utah State University had a ground based tilting filter photometer to measure the emissions at 4278Å, 4861Å, 5312Å, 5577Å and 6300Å, a fixed photometer at 3914Å and 5577Å, and a spatial scanning photometer at 3914A, 5577A and 6300A. They also provided IR radiometers at 1.5μm, 1.65μm, and 1.27μm, and a visible and IR prism interferometer-spectrometer to measure auroral spectra from 6000-9000Å and 1-3μm. The University of Michigan supplied a Fabry-Perot interferometer and a rocking filter photometer at Ester Dome for measurements at 5577Å, 6300Å, 5896Å and 7319Å. The Chatanika incoherent scatter radar was operated by SRI to provide measurements of electron density and temperature. Lockheed Missile and Space Company provided measurements from an image intensifier TV, an interferometer, a three beam photometer and a multichannel photometer.

The rocket instrumentation included an electrostatic analyzer to measure electrons with energies from ~3 to 30 keV, an energy deposition scintillator

(11) Burt, D.A. and Davis, C.S., AFCRL-TR-74-0195, Utah State University, Logan Utah, 6 (1974).

to measure the electron energy flux greater than ~3.5 keV and particle counters to measure the electron flux greater than 4.5 keV, 9 keV, 17 keV, 28 keV, 42 keV and 86 keV.

There was also a retarding potential analyzer to measure the positive ion density, a plasma frequency probe for the electron density, and a Langmuir probe to determine electron density and temperature. The positive ion and neutral composition was measured with a mass spectrometer and photometers measured visible and UV emissions at 5199A, 3466A, 3800A, 5577A, and 3914A. The infrared emissions were measured with a circular-variable interference filter spectrometer from 1.6 to 5.4μm, and two dual channel radiometers, with one verticle at 5.3μm and 4.3μm and the other 80° from the vertical at 5.3μm and 2.7μm.

4.2 Energy Deposition Scintillator Results

The ground based data[1] indicate that the rocket intercepted the arc (1/2 maximum brightness) at about 110 seconds after launch and by 120 seconds the rocket was past the 1/2 max. brightness point. The arc moved southward prior to launch and as the rocket intercepted the field lines passing through brightest region of the arc, the center of the arc moved southward very slowly. After approximately 110 seconds after launch the arc moved slowly northward until 160 seconds. The maximum arc radiance measured by the meridian scanning photometers at Ester Dome were about 50-75 kilorayleighs at 5577A°. The measurements have not been corrected for extinction or scattering by molecules and aerosols in the lower atmosphere. All sky photographs[12] taken by all sky cameras located at Poker Flat, Fort Yukon, and Ester Dome are shown in Figures 4 & 5. They indicate that from about 49 seconds before launch to at least 306 seconds after launch the arc was fairly stable. Figure 6 shows all sky photographs taken at various times with the energy flux measured by the scintillator plotted vs. time after launch below. The scintillator saturated as the rocket entered the arc region at about 90 seconds (108 km) and remained saturated until 123 seconds (143 km). As the rocket moved out of this region the energy flux decreases by over two orders of magnitude in 8 seconds (~5 km horizontal range of the rocket).

---

[12] Kofsky, I.L.; J. W. Meriwether, Jr., J. W. Shroeder, and R. B. Sluder, Data Reduction and Augoral Characterizations for ICECAP, DNA Report 3511F, Photometrics Inc., 50-84 (1975).

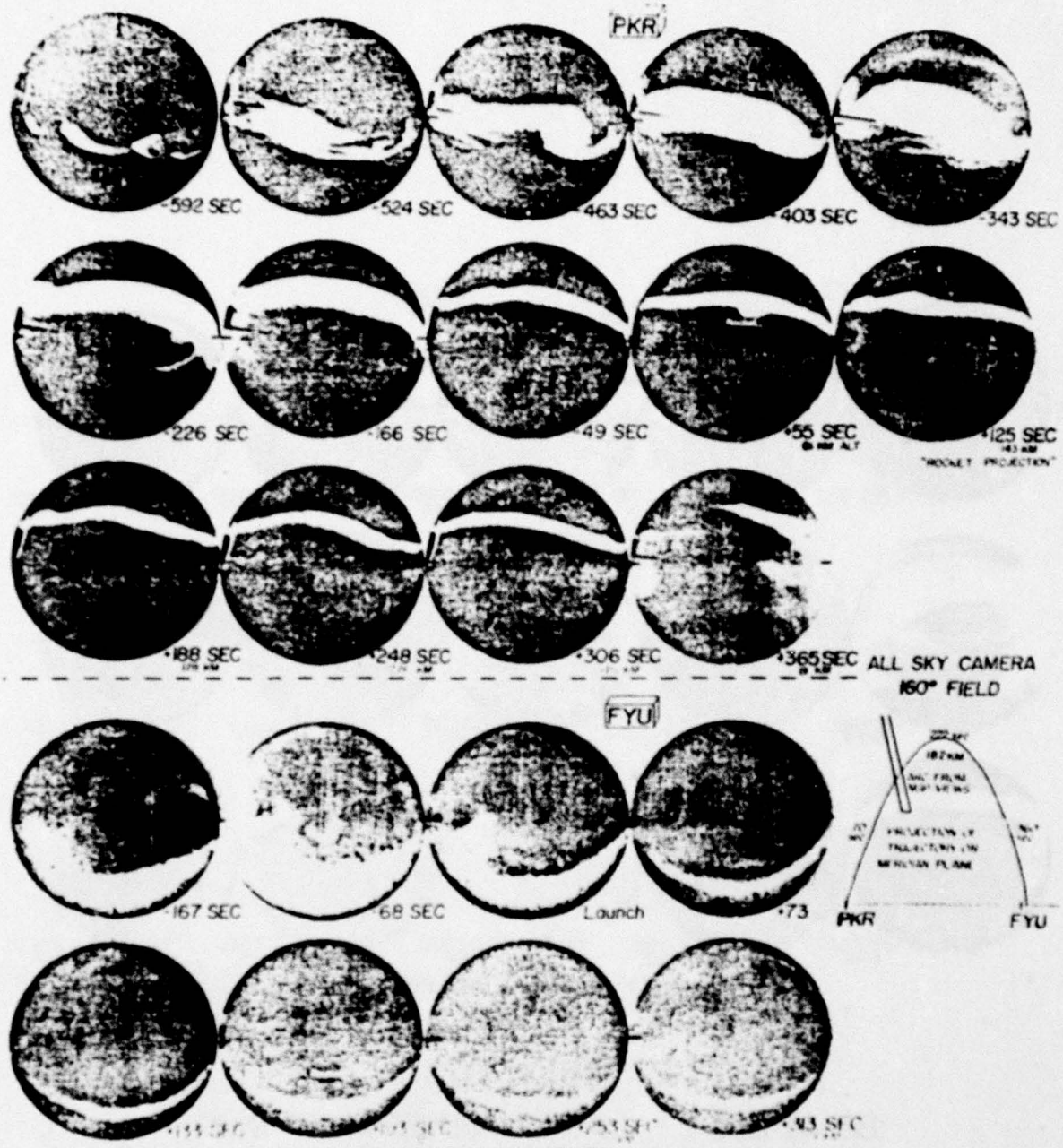

Figure 4. All-sky photographs taken at Poker Flat and Fort Yukon for the flight of Rocket A18.205-1.

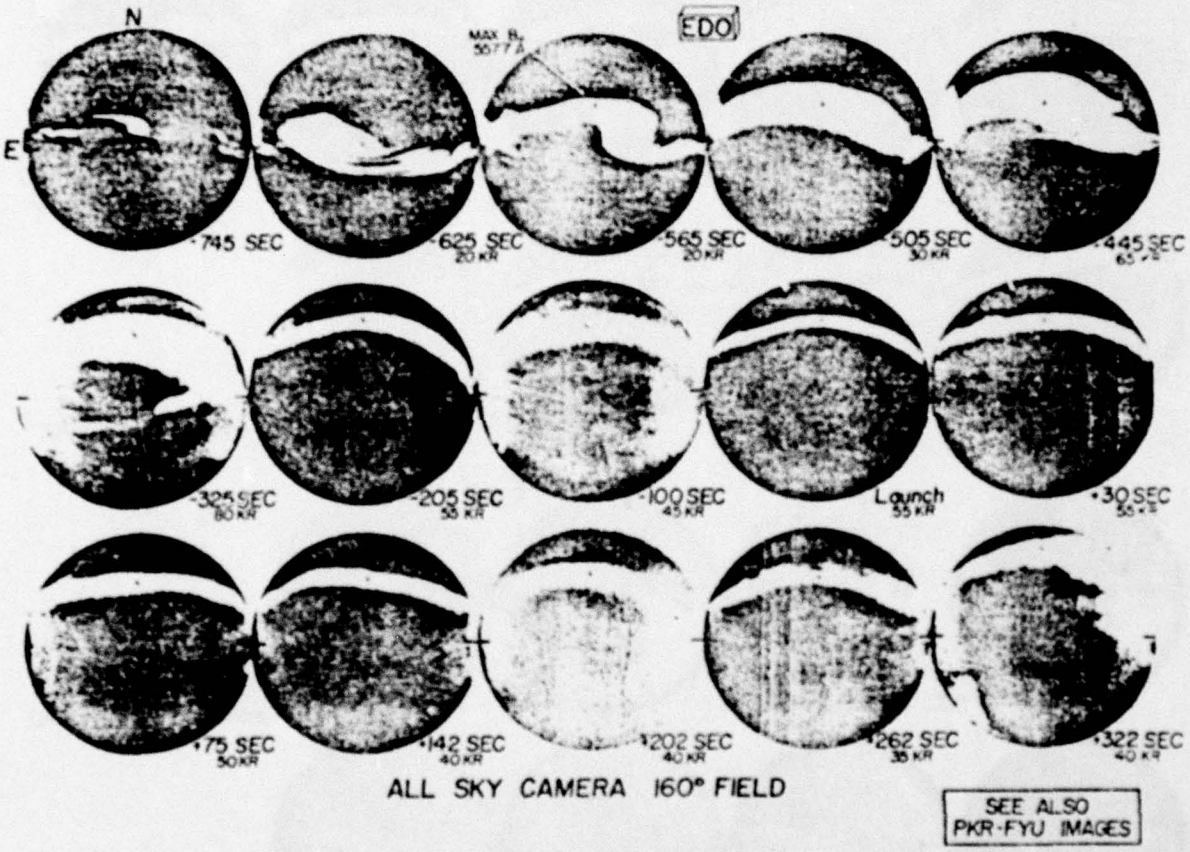

27 MARCH 1973

BB-A18.205-1 LAUNCH 09:37:45 UT SWIR
PT-A10.216-3 LAUNCH 09:38:25 UT SWIR

Figure 5. All-sky photographs taken at Ester Dome for the flight of Rocket A18.209-1.

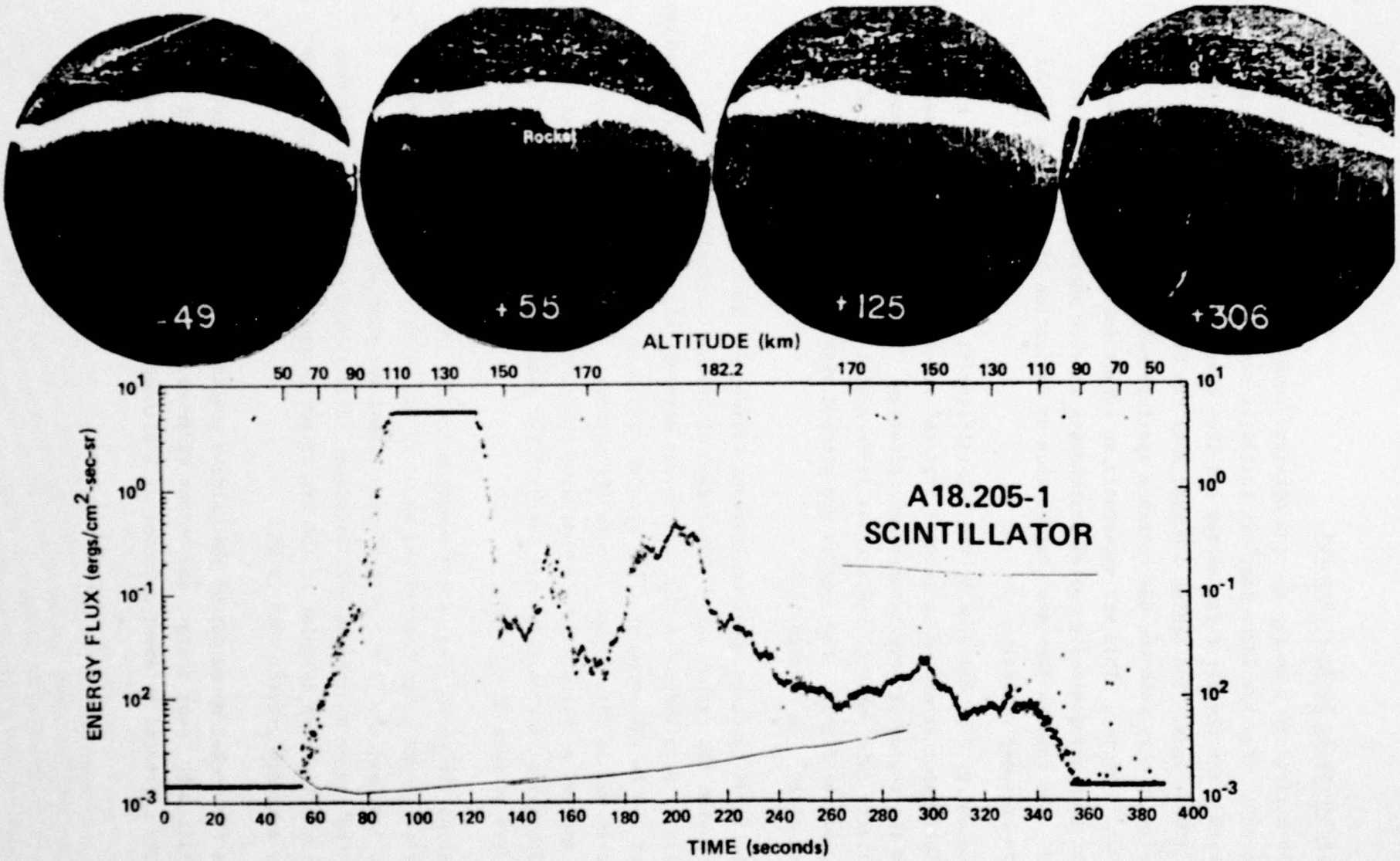

Figure 6. Energy flux measured by the scintillator on Rocket A18.205-1 and all-sky photographs taken at various times.

4.3 Electrostatic Analyzer Results

The differential energy spectra obtained from the ESA measurement are shown in Figure 7. When the instrument was initially turned on at about 90 km arcing was observed for the first few sweeps and then every few sweeps until approximately 120 seconds. The arcing occurred near the beginning of the plate voltage sweep only when the ESA entrance aperture made its minimum angle with the velocity vector. This was apparently an effect due to leakage of liquid nitrogen from cryogenically cooled instruments located above the ESA on the payload. The spectra that are plotted show no indication of arcing on either the data or sweep channels.

The energy flux measured by the scintillator is shown in the lower curve. The scintillator saturated at about 5 ergs/cm^2-sec-sr as the rocket passed through the region of most intense precipitation. The numbers on the graph of scintillator data refer to the various differential energy spectra plotted in the top of the figure. The spectra are plotted with a reference mark on each spectrum of 10^7 $(cm^2\text{-sec-sr-keV})^{-1}$.

The first measured spectrum (without arcing) was made at 95.5 seconds (114 Km) when the rocket was in the region of intense precipitation. The scintillator data indicates that the rocket entered this region (>1 erg/cm^2-sec-sr) at about 100 Km (84 seconds). The spectra remained relatively constant when the rocket was in this region (95 to 119 seconds). The spectra peaked near 17 keV and had a full width half maxima of about 11 keV. The energies at which the differential intensities were one-half the peak intensity were about 11 and 22 keV so that $\Delta E/E_c \simeq 0.66$.

During the period the rocket overflew the arc (95 to 119 seconds) the horizontal ground range covered was about 28 Km. The arc was moving south at this time and the first spectral measurement was made after the rocket was in the region of intense precipitation. Even though the rocket trajectory was not exactly perpendicular to the arc it would appear that the width of the arc was somewhat greater than 28 Km.

As the rocket moved out of the intense precipitation region, the spectral peak shifted to lower energy, and became narrower. The peak differential intensity increased by about a factor of 2 although the energy of this peak

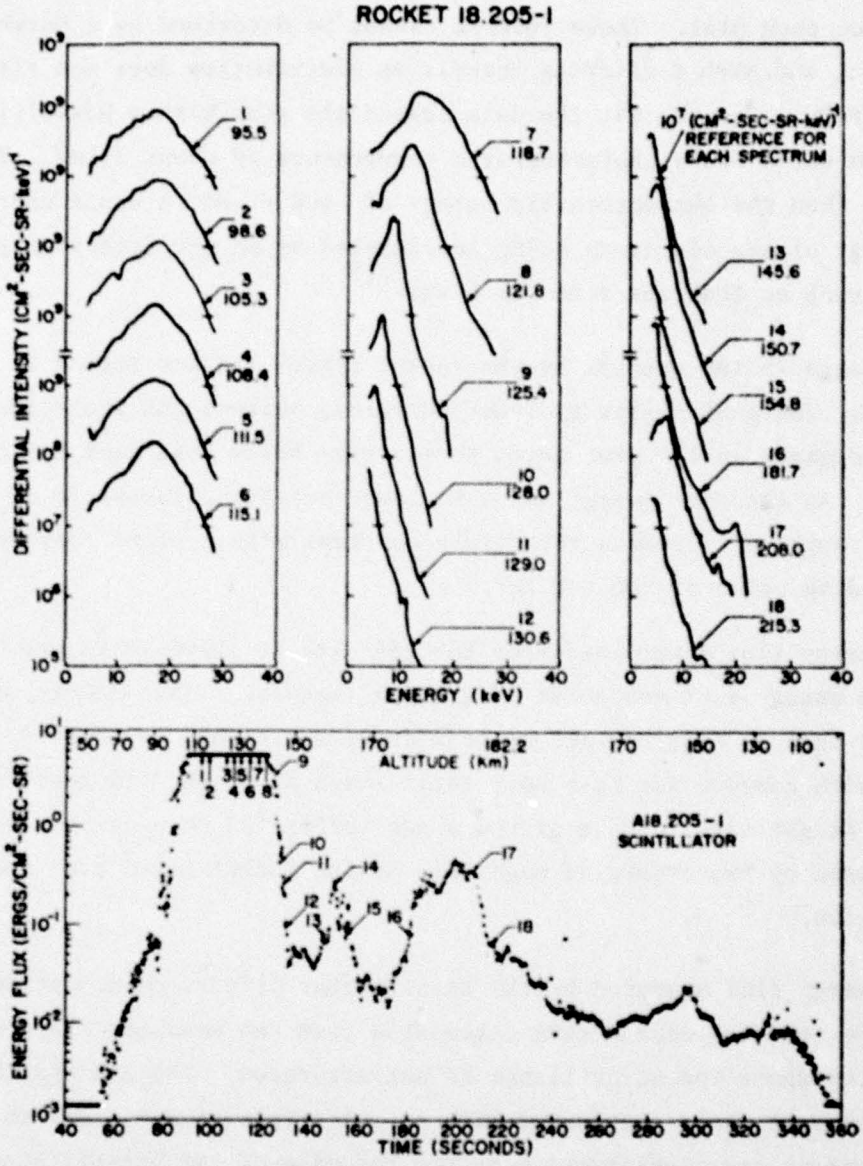

Figure 7. Electron spectra measured by the ESA on Rocket A18.205-1 for the times indicated. The times of the spectra are indicated on the scintillator data. Note the 10^7 $(cm^2\text{-sec-sr-keV})^{-1}$ reference mark for each spectrum.

shifted from 17 keV to below 3 keV. On an energy-time plot with the flux color coded this would appear as one side of an inverted 'V' structure[13].

Figure 8 shows the differential intensity of the various spectra measured in the arc region. The near constancy of the spectra in this region can be clearly seen. The time, altitude and pitch angle range of each of the spectra are listed on each plot. These spectra cannot be described by a Maxwellian distribution, and even a drifting Maxwellian distribution does not fit the data very accurately. One can fit the data beyond the peak with a Maxwellian distribution which has a characteristic temperature of about 3 keV. This is much higher than the characteristic energy of ~800 eV which would correspond to low energy plasma electrons being accelerated by an electrostatic potential in a model such as that described by Evans.[14]

The change in the spectra as the rocket leaves the arc region is shown in Figure 9. The peak shifts to lower energies, narrows and increases slightly, and then decreases as the peak moves to energies below the lower energy limit of the ESA. As the peak energy moves to lower energies, the slope of the high energy tail appears to remain relatively constant with a slope corresponding to an e-folding value of about 1 keV.

The energy flux determined from the ESA data is shown in Figure 10. The maximum energy flux was about 50 ergs/cm^2-sec-sr. The energy flux was greater than 30 ergs/cm^2-sec-sr from about 95 seconds to about 123 seconds, which corresponds to a horizontal range of 32 km. In less than 10 seconds of flight time (~10 km ground range) after 123 seconds the energy flux decreased by two orders of magnitude as the rocket moved away from the arc region.

The energy flux measured by the scintillator differs by almost an order of magnitude from the energy flux calculated from the measured ESA spectrum in the region where the scintillator is not saturated. The ESA and the scintillator were cross-calibrated with an α-particle source prior to flight but there was no cross-calibration of the response of the scintillator to low energy electrons. It appears that in regions where the ESA spectra

---

[13] Frank, L. A. and K. L. Ackerson, J. Geophys. Res. 76, 3612 (1971).

[14] Evans, D. S., J. Geophys. Res., 79, 2853, 1974.

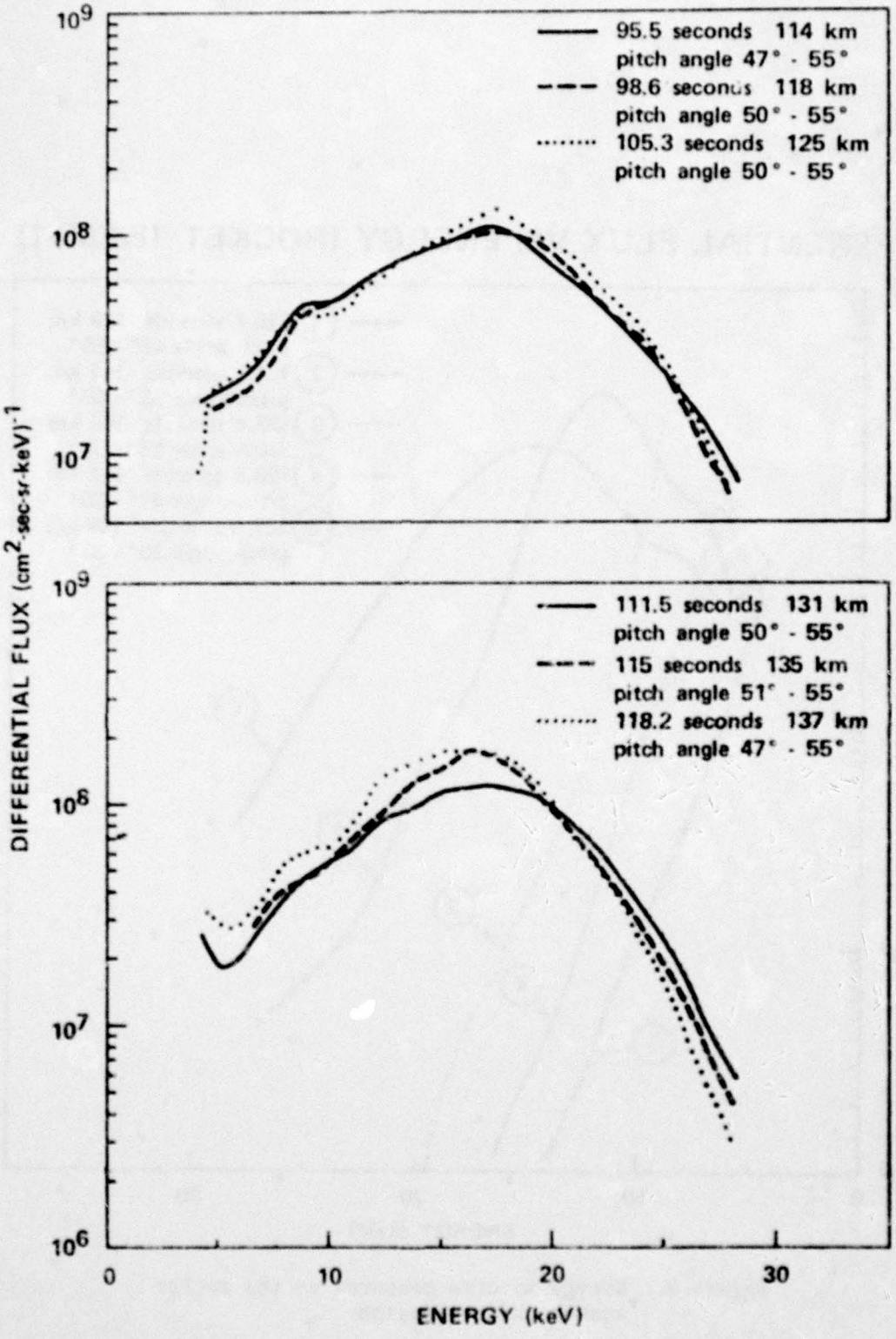

Figure 8. Energy spectra measured in the auroral arc.

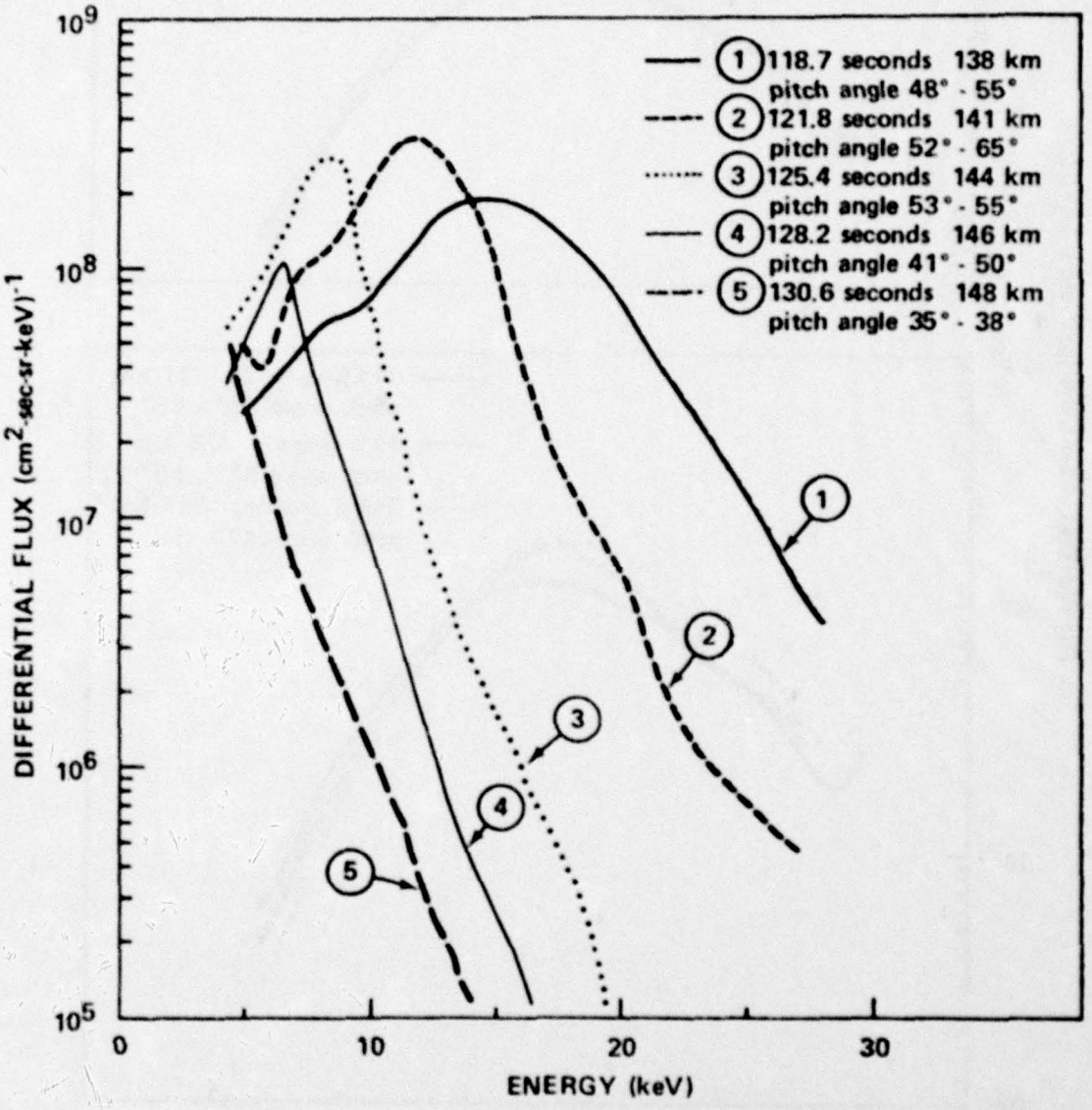

Figure 9. Energy spectra measured as the rocket leaves the arc region.

indicate that most of the energy is being deposited by lower energy electrons that there is severe disagreement. Figure 11 is the energy flux determined by using the spectra measured by the ESA and calculating the energy flux that would be measured by the scintillator taking into account the energy lost in aluminum foil on the scintillator. There is agreement within a factor of two between this calcualtion and the energy flux measured by the scintillator. The remaining discrepancy could be due to a thicker aluminum foil over the scintillator than indicated in the specifications.

In Figure 10 it can be seen that the rocket traversed the region of two smaller arcs at about 150 seconds and 200 seconds both of which had energy fluxes of about 2 ergs/cm^2-sec-sr. The peak differential intensity occurs at approximately 5 keV (10^8 electrons/cm^2-sec-sr-keV) and 7 keV (0.4×10^8 electrons/cm^2-sec-sr-keV). Beyond 240 seconds the measured differential flux is close to the noise level of the ESA and these data have been deleted.

The total flux of electrons obtained by integrating differential energy was approximately 10^9 electrons/cm^2-sec-sr in the main aurora (90 to 120 seconds) and was 2×10^8 electrons/cm^2-sec-sr in the two smaller auroral bands measured at 150 seconds and 200 seconds.

4.4 Pitch Angle Distribution

Since the rocket was oriented to be within a few degrees of vertical, the pitch angle coverage was limited. The rocket made an angle of approximately ten degrees with the magnetic field over most of the flight so that the ESA measurement generally covered pitch angles from 35° to 55° while the scintillator ranged from 45° to 55°. In the region of the most intense flux the scintillator was saturated and the ESA spectra in this region (where no evidence of arcing was observed) generally covered only pitch angles between 45° and 55°. In this very limited range there was no evidence for any variation in the differential intensity with pitch angle. Outside of this region (before ~90 seconds and after ~125 seconds) the scintillator is not saturated and plots of the flux vs. pitch angle have been made in regions where the flux is not making a rapid temporal or spatial change in one spin period. Figure 12 is a sample of these plots made at 76 and 133 seconds and

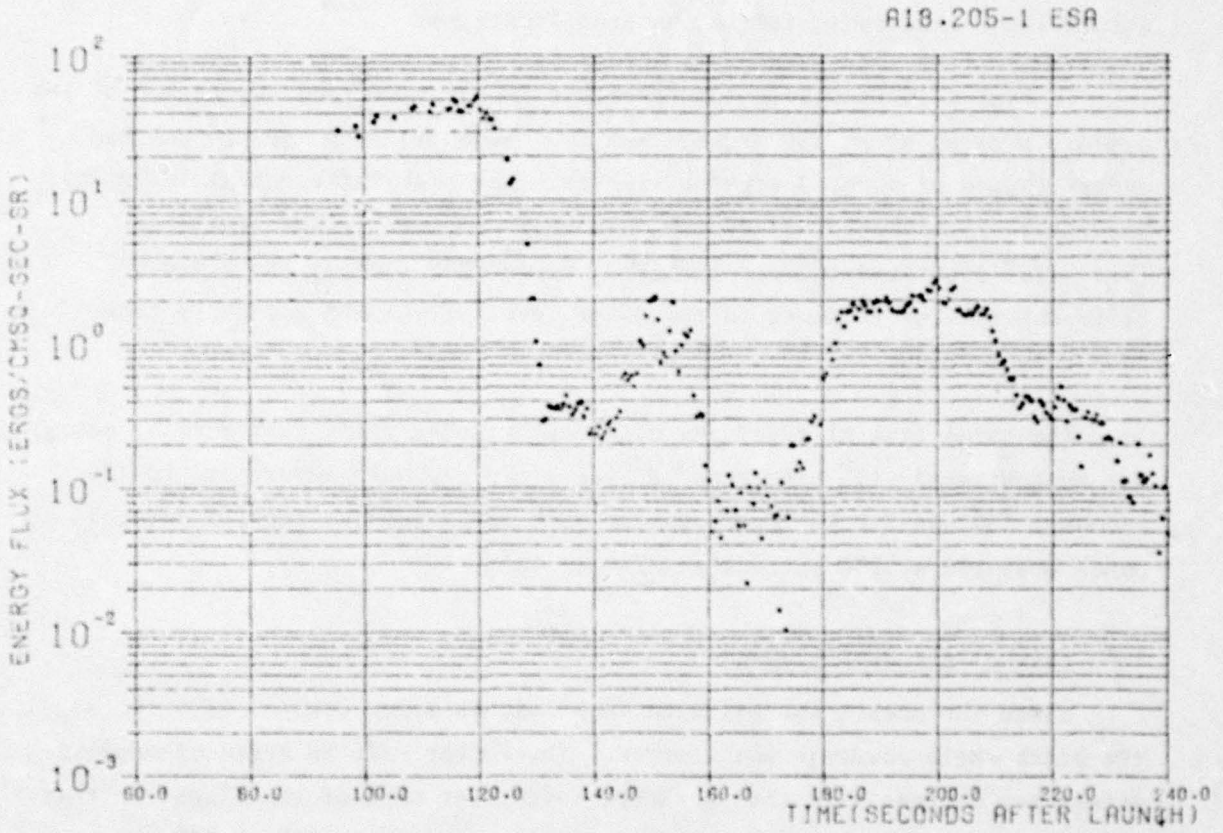

Figure 10. Energy flux calculated from the measured energy spectra for Rocket A18.205-1.

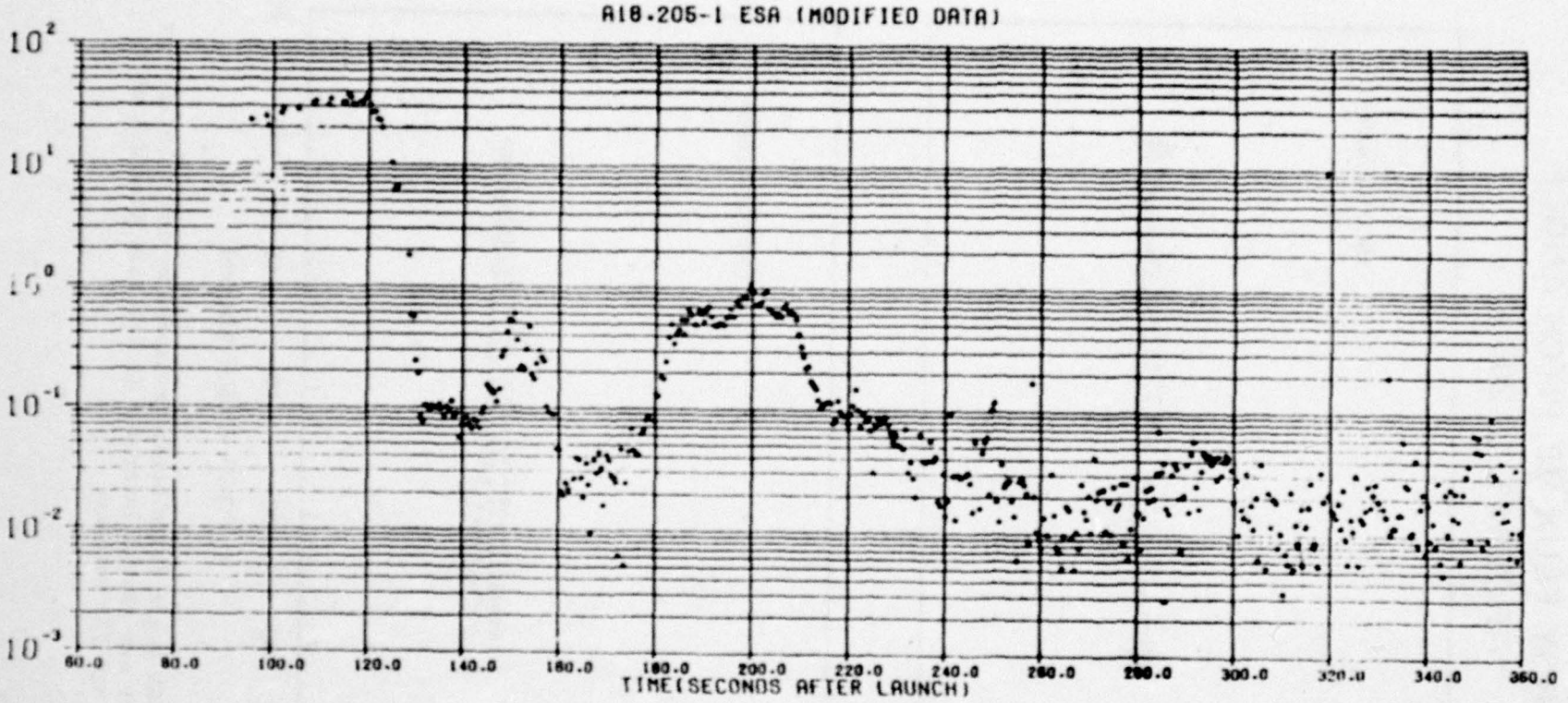

Figure 11. Energy flux that should be measured by the scintillator as calculated from the measured energy spectra.

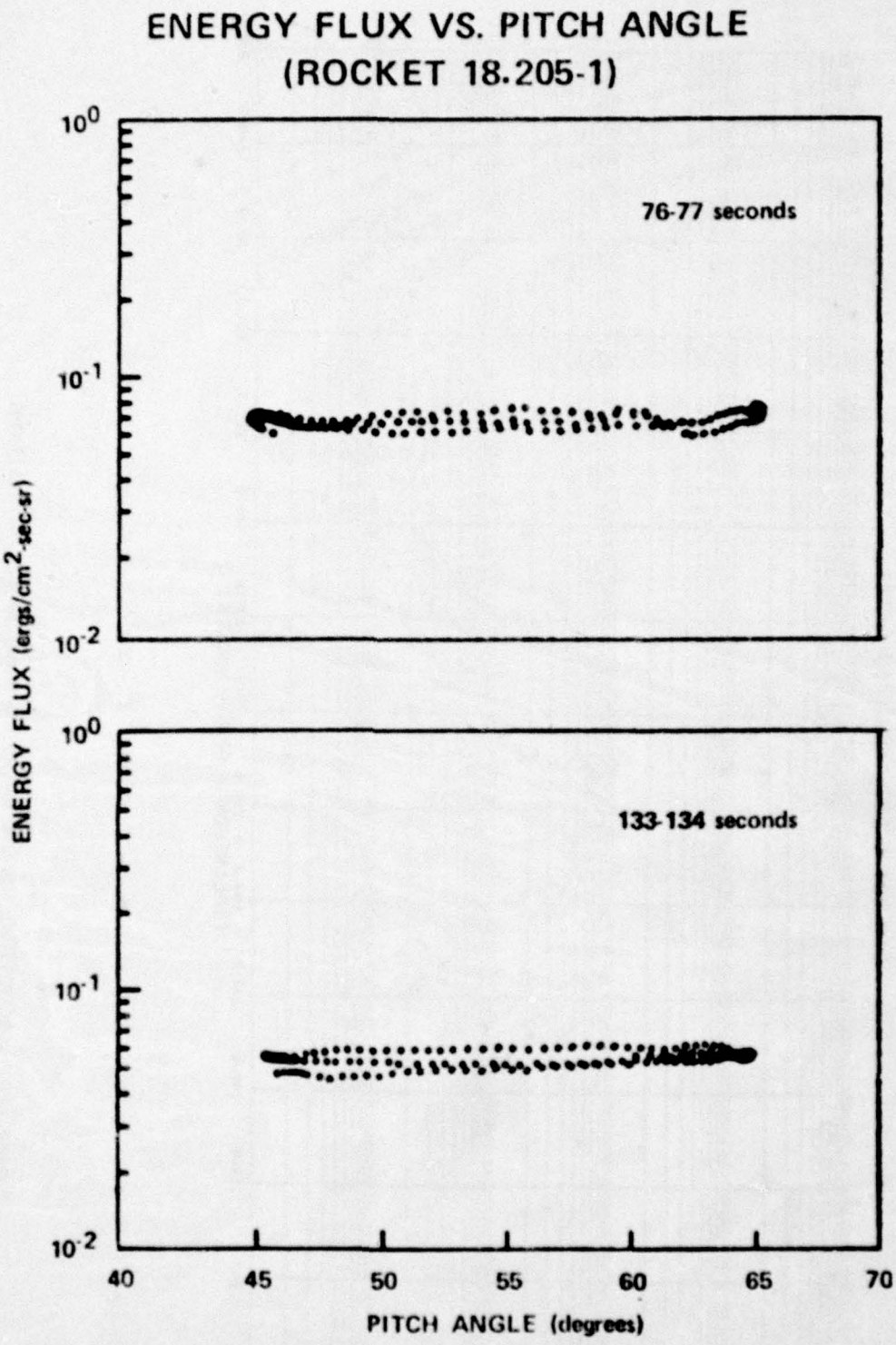

Figure 12. Pitch angle distribution measured by the scintillator over one second intervals (1 1/2 spin periods) at 76 and 133 seconds.

covering about one second or approximately 1 1/2 spin periods. These plots indicate that the flux is isotropic over this limited pitch angle range. These plots are typical of plots made throughout the flight in regions where there were no temporal or spatial changes in a spin period (about 1/2 second). The ESA data also indicates that the flux is isotropic over the pitch angle range from 35° to 55°, although in this case spatial, temporal and spectral changes have to be separated and the differential intensity at a given energy is measured only once every one-half second.

4.5 Ion-electron Production Rate, Electron Density and 3914 Emission Calculations

The differential intensity measured by the ESA was used to calculate the ion-electron production rate using the technique described by Rees[15]. The spectra measured at 134 km was used to calculate the production rate below this altitude. The spectrum was assumed to be isotropic over the upper half plane and was integrated over the upper-half plane (by multiplying $\frac{dJ}{dEd\Omega}$ by π. Rees' cosine dependent case was used since this is equivalent to an electron flux which is isotropic over the downward hemisphere[16]. The production rate as a function of altitude is shown in Figure 13. If one integrates the production rate as a function of altitude from 130 km down to the rocket altitude and uses the relationship that 0.6 ergs/cm^2-sec is equivalent to 0.5 kilorayleighs of 3914Å radiation[17,18] one obtains the 3914Å radiation that would be measured by a vertical looking photometer. A comparison of the calculated 3914Å emission and the 3914 emission measured by a vertical looking photometer as a function of altitude is shown in Figure 14.

Below about 110 km the rocket is not in the region of the intense portion of the auroral arc so that the calculated emission, which is based on the auroral electron flux measured in the arc, does not agree with the measurement. Above 110 km the photometer is observing the 3914Å emission above the arc and

---

[15] Rees, M., Planet. Space Sci., 11, 1209 (1963).

[16] Berger, M. J., S. M. Seltzer and K. Maeda, J. Atmos. Terr. Phys., 32, 1015, 1970.

[17] Dalgarno, A., I. D. Latimer, and J. W. McConkey, Planet. Space Sci., 13, 1008 (1965).

[18] McConkey, J. W., J. M. Woolsey, D. J. Burns, Planet. Space Sci., 15, 1332 (1967).

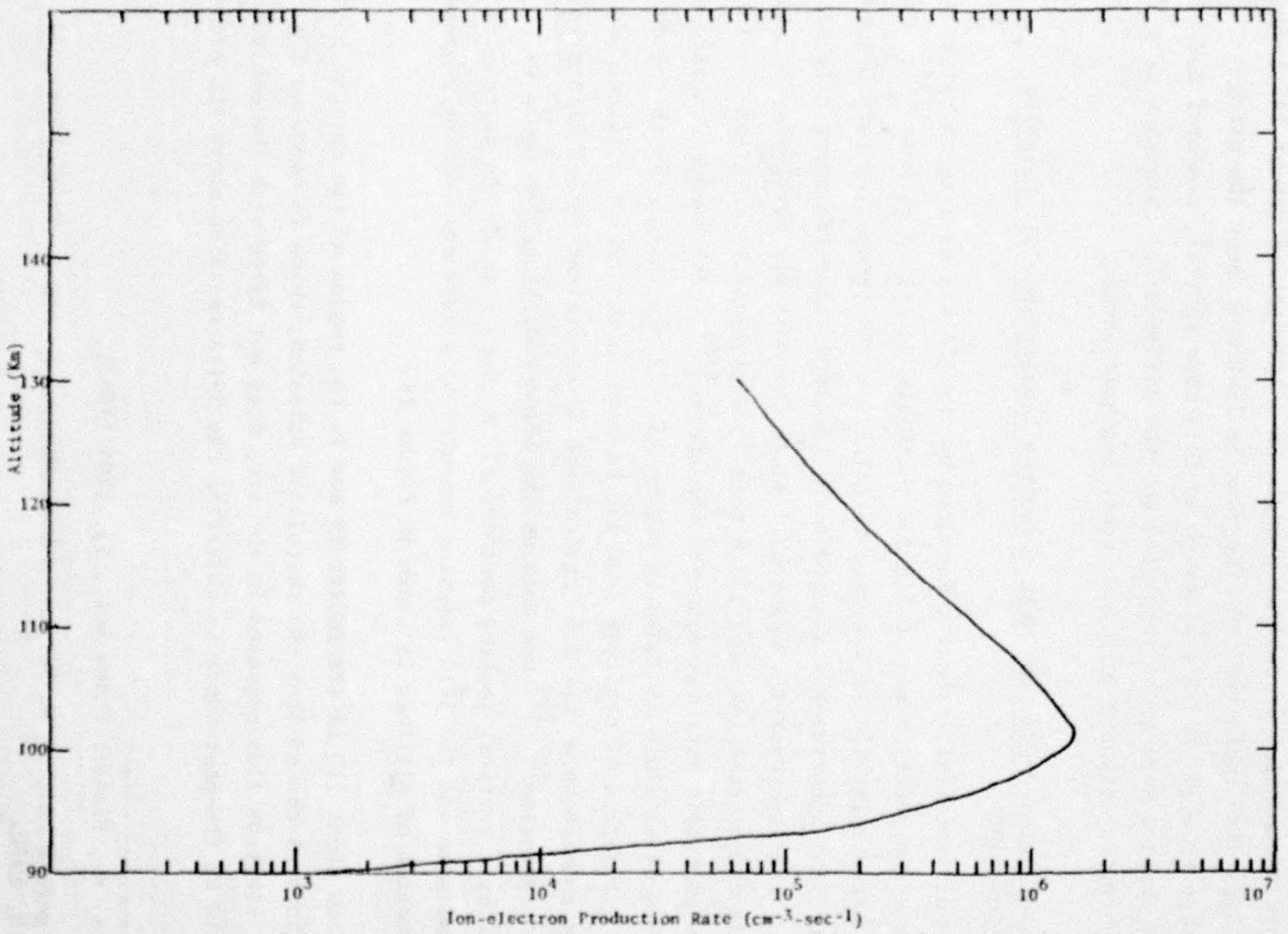

Figure 13. Ion-electron production rate calculated from the measured electron spectra.

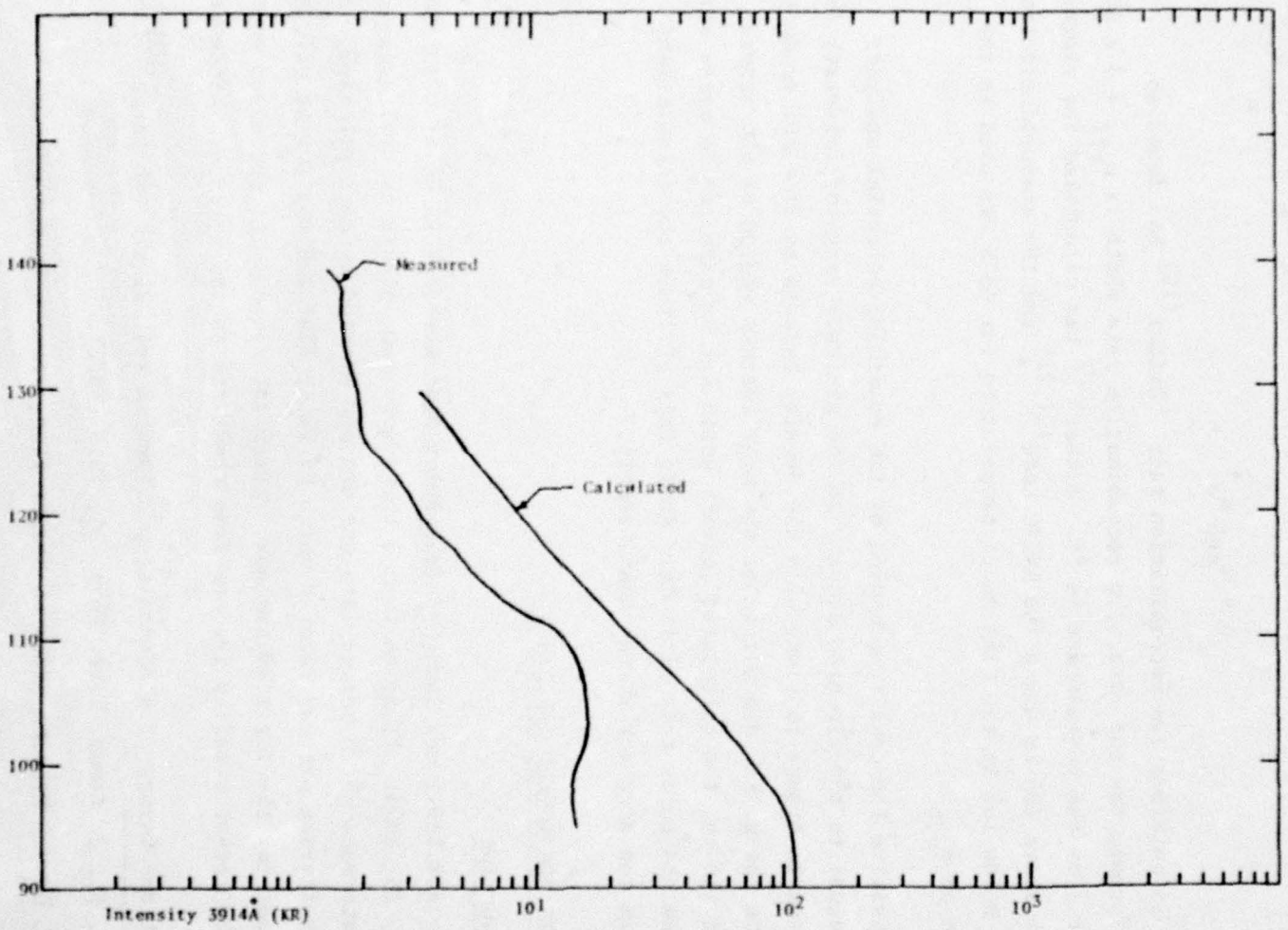

Figure 14. 3914Å radiation measured by the vertical photometer and calculated from the production rate.

there is agreement within a factor of two. This is slightly greater than the absolute calibration accuracy of the ESA which is about ±50%. The production rate (q) may also be used to calculate the electron density n_e from the equation

$$q = \alpha_{eff} n_e^2$$

where α_{eff} is an effective recombination rate. Swider[19] has found an empirical formula for the effective recombination rate which is $\alpha_{eff} = 3 \times 10^{-7} (\frac{300}{T})$ where T is the temperature in °K. Archer[20] has calculated the electron temperature above 105 km using the ARTIC code[21,22] and the measured electron spectra.† Below 105 km the CIRA model temperature for 60°N was used in the calculation of α_{eff}.

The positive ion density measured by the retarding potential analyzer (which is equal to the electron density in the altitude range of interest) is shown plotted in Figure 15 along with the density calculated from the production rate. Since the rocket did not enter the most intense region of the aurora until about 110 km, the calculated density would not be expected to agree with the measurements below this altitude. Above this altitude the calculations agree within the accuracy of the measurements.

5.0 RESULTS FOR ROCKET A18.219-1

5.1 Introduction

Rocket A18.219-1 was launched from Poker Flat Research Range at 07:38:30 UT on February 25, 1974. Prior to launch there were two intense auroral arcs moving equatorward which merged into one arc and started to move poleward. At launch this intense arc was located north of Poker Flat and was moving poleward at 1/2 km/sec for the first 80 seconds. After 140 seconds the arc moved equatorward and the rocket overflew the arc from about 160 to 180 seconds. After 210 seconds

† Note that the values of electron temperature in ref. 21 are too large[23].

[19] Swider, W., J. Atmos. Terr. Phys. 34, 1615 (1972).

[20] Archer, D. H., Mission Research Corporation, Private Communication.

[21] Archer, D. H. and P. W. Tarr, Aurora Simulation Studies, DNA 3567T, HAES Report No. 6, MRC-R-152, Mission Research Corporation; 1974.

[22] Tarr, P. W., D. H. Archer, N. G. Utterback, Studies of Auroral Simulation, DNA 3297F, MRC-R-122, Mission Research Corp., 1974.

[23] Tarr, P. W. and D. H. Archer, Auroral Simulation Studies in Support of ICECAP and EXCEDE, DNA 3785F, MRC-R-211, Mission Research Corporation, 1975.

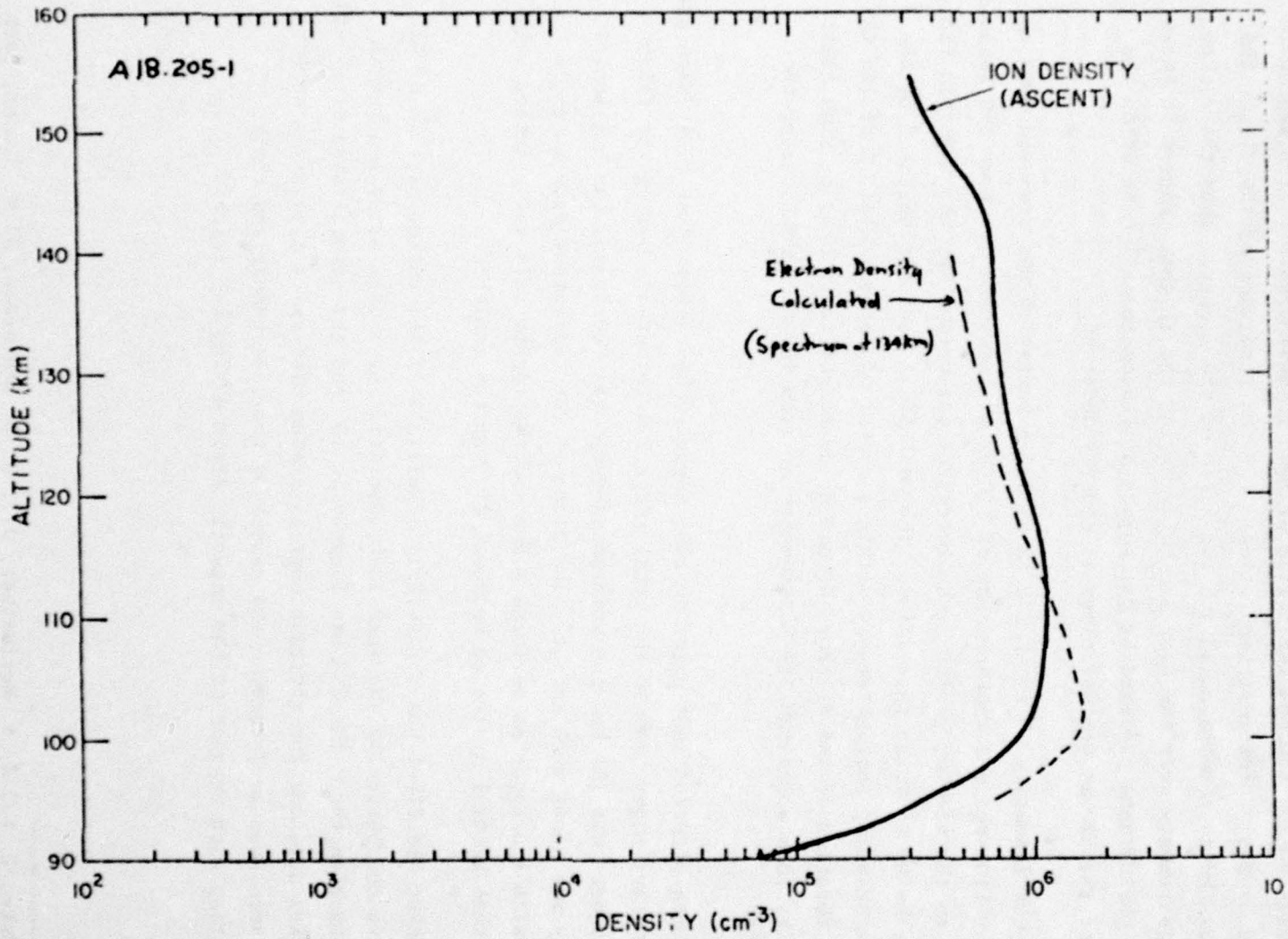

Figure 15. Positive ion density measured by the RPA compared with the density calculated from the production rate.

the arc again reversed direction as a westward surge developed, and moved poleward and appeared to broaden. The arc caught up with the rocket and from about 260 seconds to 300 seconds the region of most intense precipitation was again measured by the rocket instrumentation. For the remainder of the flight the arc continued to move poleward and was north of the rocket. Thus the rocket made measurements over the same arc twice during the flight. Figure 16 shows all-sky photographs prepared by Dr. Kofsky of Photometrics[24] in which the motion of the arc at various times is clearly observed.

A peak intensity of about 200 KR of 5577Å radiation was measured from the ground at 110 secs and another peak of 280 KR was measured at about 290 seconds but due to the viewing geometry the intensity measured along the magnetic field line may be up to twice this value. The peak 5577Å radiance measured by the meridian scanning photometer was within a factor of approximately 2 of 125 KR for the duration of the flight. Ground based measurements made by Utah State University show a maximum 3194Å intensity of from 100 to 200 KR during the flight[25].

Launch occurred just prior to 600γ negative bay observed at Fort Yukon and the planetary index, Kp and the total index K were both 4+ during the flight. Rocket apogee was 195 km, the horizontal range was 100 km and the horizontal velocity was about 0.25 km/sec. The plane of the trajectory made an angle of 16° with the magnetic meridian plane and the rocket axis was oriented with an attitude control system to be about 4° from the zenith.

Rocket A18.219-1 was essentially a reflight of the rocket payload of A18.205-1 and contained basically the same instrumentation with only minor changes in filter wavelengths. The ESA was located at 45° and the scintillator at 55° to the rocket axis and the attitude control system along with a magnetic aspect sensor were used to determine the aspect of the instruments and their orientation with respect to the magnetic field during the flight.

---

(24) Kofsky, I. L., J. W. Meriwether, Jr., J. W. Schroeder, R. B. Sluder, Data Reduction and Auroral Characterizations for ICECAP, DAN 3511F, Photometrics Inc. (1975).

(25) Bell, R. J., editor, Ground Support Data in Support of Black Brant 18.219-1 Flight, Utah State University (1974).

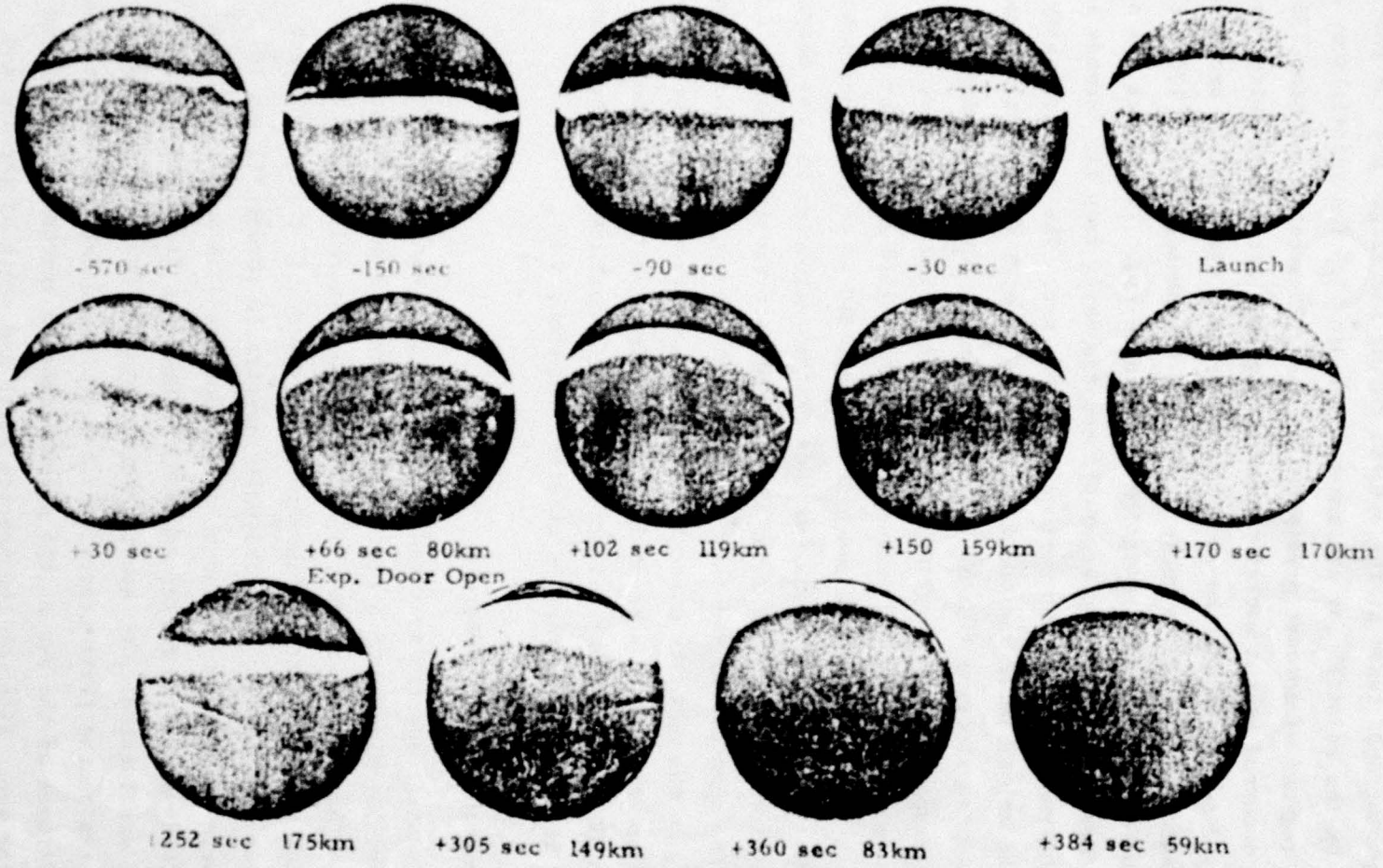

Figure 16. All-sky photographs during the flight of Rocket A18.219-1.

5.2 Energy Deposition Scintillator Results

All-sky photographs taken at three times during the flight and the energy flux measured by the scintillator are shown in Figure 17. The scintillator data shows the two regions of intense precipitation near 170 seconds and near 285 seconds which occurred as the rocket passed through the arc region twice, once as the arc moved southward and the rocket northward and again as the arc moved rapidly northward and passed the rocket. The all-sky photographs at 170, 252 and 285 seconds indicate the northward motion of a single arc. The rocket was south of the arc before 155 seconds and after 315 seconds, while from 185 seconds to 265 seconds the rocket was on the north side of the arc. The peak intensity measured by the scintillator was about 120 ergs/cm^2-sec-sr for both traversals of the arc. If the electron flux is isotropic over the downward hemisphere this would correspond to an energy deposition of about 380 erg/cm^2-sec and to a 3914Å radiance of about 314 KR (measured along the field line). The side looking detectors measured a peak radiance of about 310 KR on upleg portion of the trajectory. Although the peak radiance of the photometer was not measured at the same time as the particle data, it does indicate the approximate intensity of the aurora. In the first pass through the arc region the auroral arc was moving in the opposite direction from the rocket, while in the second traversal the arc and rocket were moving in the same direction. Without knowing the velocity of the auroral arc one can only conclude that the width of the arc in the first traversal is greater than about 5 km.

5.2.1 Electrostatic Analyzer Results

The differential spectra measured at various times during the flight are shown in Figure 18, along with a plot of the energy flux measured by the scintillator. The times at which the spectra were measured is indicated on the energy flux curve. Spectra 1 through 6 and spectra 1′ through 6′ were measured on the south side of the arc while spectra 10 through 12 and 10′ through 12′ were measured on the north side. Spectra 7, 8 and 9 and 7′, 8′ and 9′ were observed as the rocket crossed the magnetic field lines along which the arc was located. The spectra were chosen so that the unprimed numbered spectra on the first crossing of the arc would correspond to the same structural features of the arc as the primed numbered spectra on the second crossing of the arc. Although the spectra north and south of the arc and

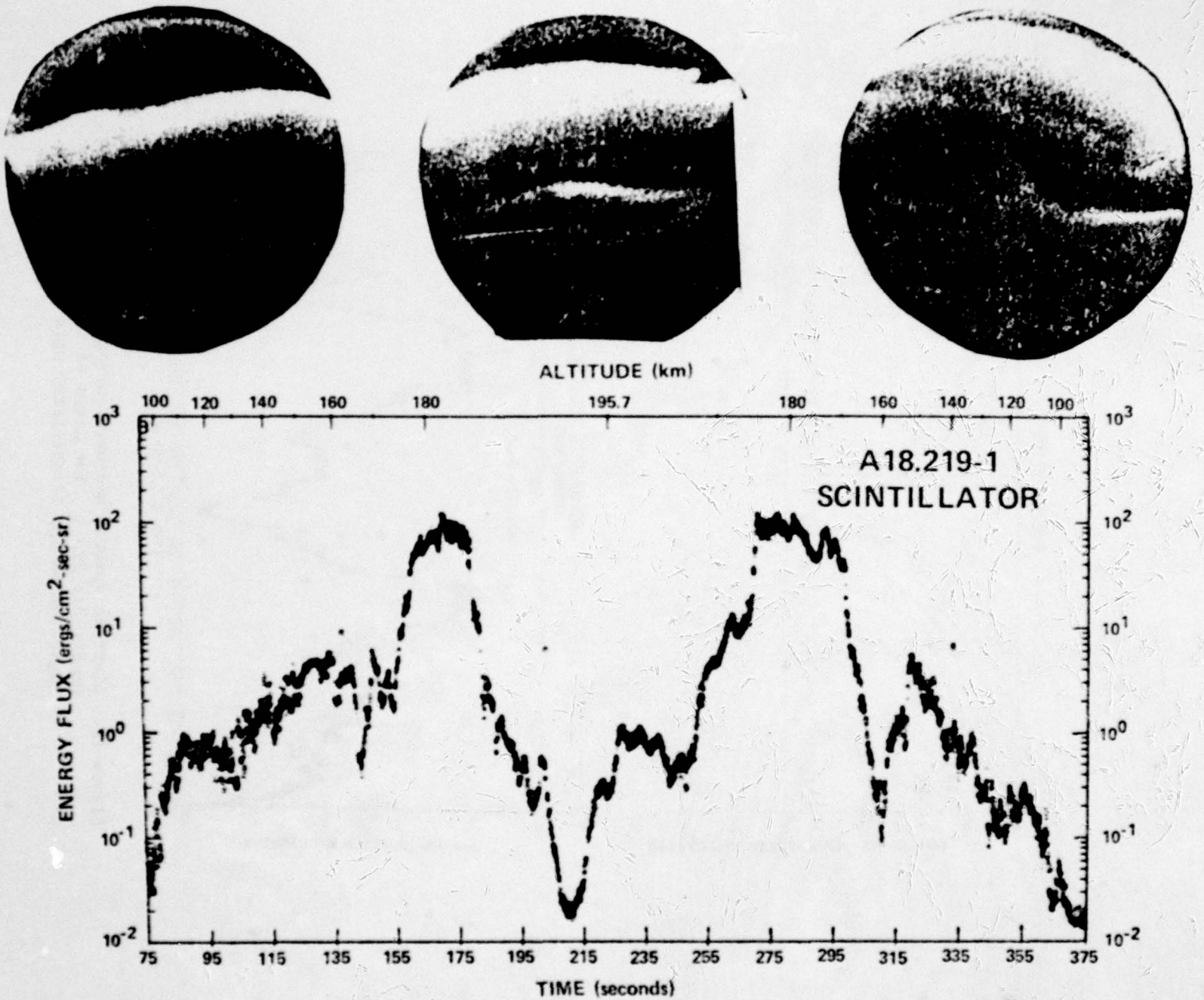

Figure 17. Energy flux measured by the scintillator on Rocket A18.219-1.

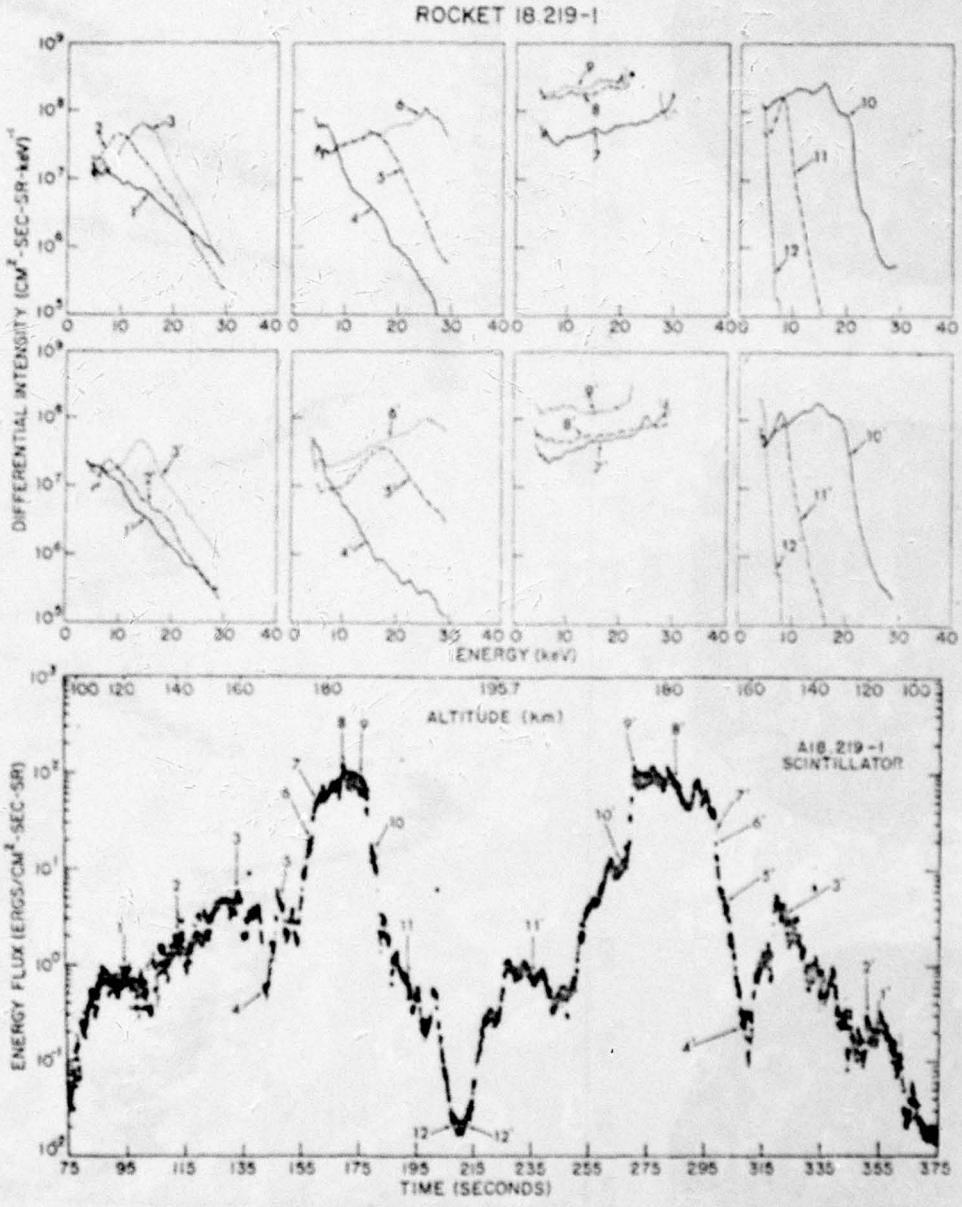

Figure 18. Electron spectra measured during the flight of Rocket A18.219-1. The times of the spectra are indicated on the scintillator data.

in the arc region are considerably different from each other, there is a remarkable consistency of the spectra measured at corresponding locations on each crossing of the arc. Each unprimed numbered spectrum is close to its primed counterpart spectrum in shape and intensity and in its location relative to the center of the arc, although they are measured up to 4 1/2 minutes apart.

The spectra measured on the southern edge of the arc are relatively hard, as shown by spectra 1 and 1′, and from 3 to 30 keV are approximately exponential in shape with an e-folding value (for spectrum 1) of approximately 6.5 keV. As one moves closer to the center of the arc the spectra develop a peak (2 and 2′) which shifts to higher energy (about 15 keV) at 3 and 3′. There is little change in peak intensity from spectrum 2 to 3 and in this region an inverted "V" structure would be observed on an energy-time plot with the intensity color coded. In region 4 (4′) there is an abrupt decrease in the energy flux (to about 0.5 ergs/cm^2-sec-sr) and the peak differential intensity shifts to lower energies (below 8 keV) with an approximately exponential fall off with energy beyond the peak energy (e-folding value of ~3.5 keV). Spectrum 5 (5′) measured as one moves toward the center of the arc shows the peak moving to higher energies (about 15 keV), but (for spectrum 5) the differential intensity at 3 keV is only about a factor of 2 less than the measured peak differential intensity. Beyond the peak, the differential intensity decreases exponentially with an e-folding value of ~2.6 keV. As the rocket moved into the center of the arc, the energy flux increased rapidly and the peak differential intensity (6 and 6′) shifted to higher energies (~26 keV). The differential intensity at 3 keV is only a factor of 3 less than that measured at the peak for spectra 6 and 6′ (which are nearly the same). The lower energy portion of spectrum 6 is nearly identical to the intensity measured below the peak of spectrum 5. It would appear that as the peak moves to higher energy, the differential intensity at lower energies remains essentially unchanged. Spectra 7′, 8′and 9′and corresponding and 9′ were measured in the region of most intense precipitation. Spectrum 7 (and its nearly identical counterpart 7′) show that the peak has moved to higher energies, beyond 30 keV (the upper energy limit of the instrument) while the low energy part of the spectrum is nearly unchanged from spectrum 6 for energies less than the peak. Below about 6.5 keV

spectra 7 and 7′ both show the differential intensity increasing with decreasing energy. From 6 keV to 28 keV there is an approximately exponential increase in the differential intensity with an e-folding value of about 17 keV, and the intensity increases by about a factor of 2 from 28 to 30 keV. The spectra measured in the center of the arc saturated the amplifier at higher energies for both traversals of the arc and it appears that there was an appreciable electron flux beyond 30 keV so that a complete description of the spectra is not possible. (However, the ESA appears to have measured most of the energy flux as will be seen later.) Spectrum 8 is shown to only 22 keV because the amplifier saturated but spectrum 8′ (which has the same shape as spectrum 8) is lower in intensity by a factor of 3 and it is shown to 30 keV. The peak in the spectra appears to be beyond these energy limits. The measured intensity changes by less than a factor of two, between 3 and 20 keV for spectrum 8 and between 3 and 30 keV for spectrum 8′. The intensity of spectrum 8′ is about a factor of 2 greater than that of spectrum 7′ at the lower energies but for spectrum 8 it is about a factor of 4 greater than the intensity of spectrum 7 at all measured energies. Spectra 9 and 9′ were measured at the northern edge of the arc and they both indicate a peak in the differential intensity between 20 and 27 keV (the amplifier has saturated in this region) and were relatively flat between 3 and 20 keV. Below 20 keV spectra 8 and 9 are nearly the same while spectrum 9′ is a factor of 2 greater than 8′ over this energy range. Spectra 10 and 10′ were measured on the north side of the arc. The spectra are quite similar and show that the peak has moved to a lower energy (~15 keV) with a very sharp fall off beyond the peak energy (e-folding value of ~1 keV) and about a factor of 3 change in intensity from 3 keV to the peak energy. Further measurements on the north side of the arc show that the total energy flux decreased as the peak differential intensity shifted to lower energy.

Spectra 11 and 11′ show that the peak intensity was not changing appreciably as the peak moved to lower energy (which is characteristic of an inverted "V" on an energy-time plot) and an almost exponential fall-off beyond the peak energy with an e-folding energy of about 1 keV. The peak differential intensity shifted to lower energies and eventually the peak was below the lower energy limit (~3 keV) of the instrument as shown in spectra 12 and 12′. The fall off with energy beyond the peak may be characterized in this case by an exponential with an e-folding value of about 0.5 keV which is somewhat less than observed for spectra 10(10′) and 11(11′).

It appears that changes in the spectra observed as the rocket moved across the arc region are primarily spatial since the corresponding spectra measured (at equivalent total energy levels) in the two crossings of the arc are quite similar, and various features appear to be consistent across the arc. The slope of the spectra beyond the peak appear to be harder (e-folding ~3 to 6 keV) on the south side of the arc than on the north side (e-folding ~0.5-1 keV). On both sides of the arc the spectra measured near the arc relatively flat (within a factor of 2 to 3) from the lowest measured energy (~3 keV) to the peak. The peak moves to higher energy with little change in differential intensity as the one moves toward the center of the arc from either side, which is characteristic of an inverted "V" (as observed on an energy-time plot). The basic structure and total energy of the arc seems to have remained approximately the same in the two transversals of the arc which occurred about 2 minutes apart. The arc appears to have a more limited spatial extent north of the region of peak energy flux as compared with the region south of the peak, but this may be an artifact due to the motion of the arc.

The total energy deposited has been calculated from the differential energy spectra measured by the ESA, and is shown as a function of time in Figure 19. The total energy measured in the first crossing of the arc is about 200 ergs/ cm^2-sec-sr and is about twice that measured by the scintillator although the complete spectra were not measured by the ESA due to the high energy cut-off (30 keV) and the saturation of the ESA amplifier at high flux. In the second traversal of the arc the total energy measured by the ESA is less than from the first crossing while the scintillator is about the same for both arc traversals. This indicates that a greater portion of the total energy deposited is not being measured by the ESA in the second crossing (as compared with the first crossing) due to the aforementioned effects. Figure 20 shows the result of calculating the energy flux that would be measured by the scintillator as a result of the energy lost in the aluminum foil covering the scintillator and assuming for the incident spectra, the spectra measured by the electrostatic analyzer. Figure 21 is a plot of the scintillator data to the same scale. The energy flux calculated from the ESA data agrees within a factor of 2 to 3 with the data measured by the scintillator.

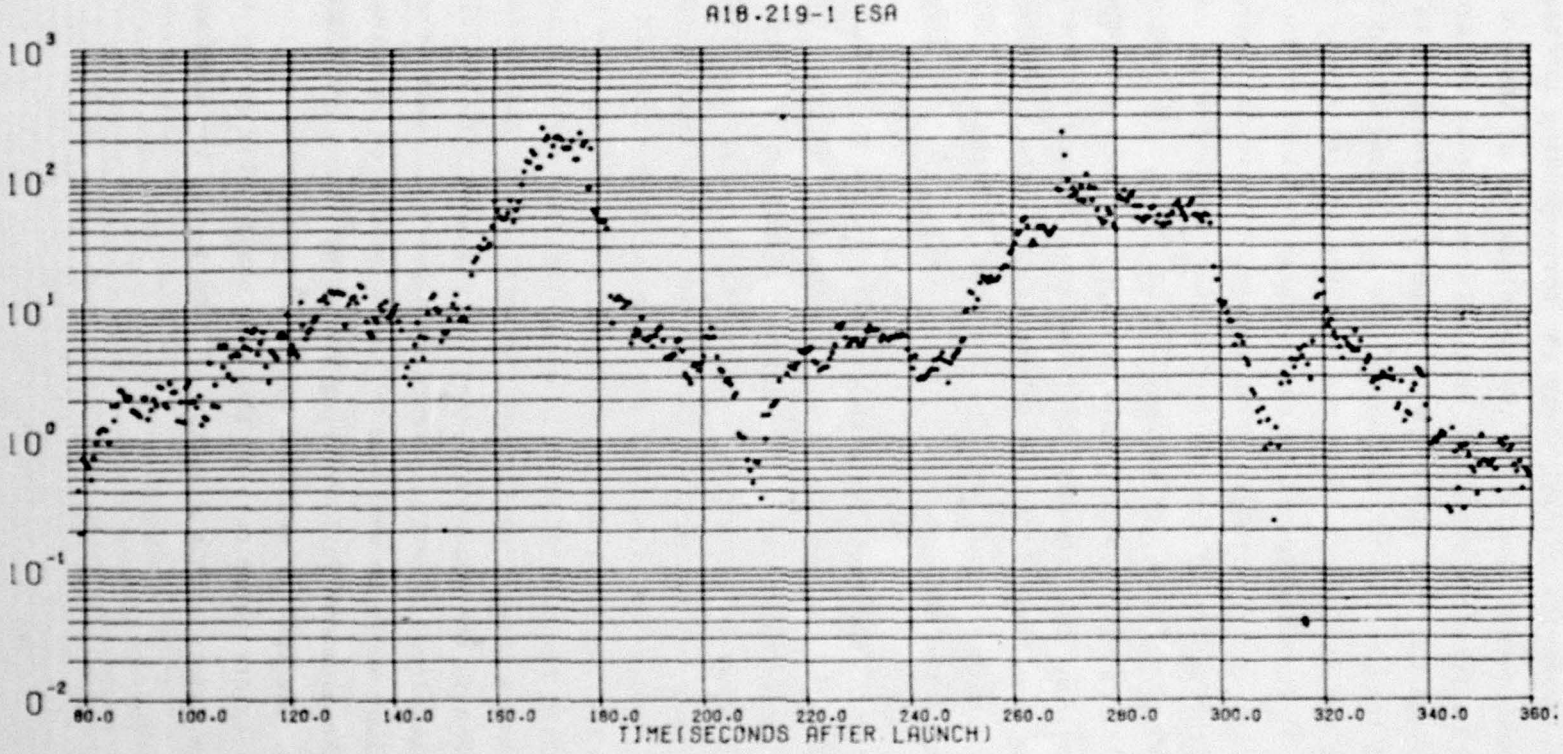

Figure 19. Energy flux calculated from the measured energy spectra for Rocket A18.219-1.

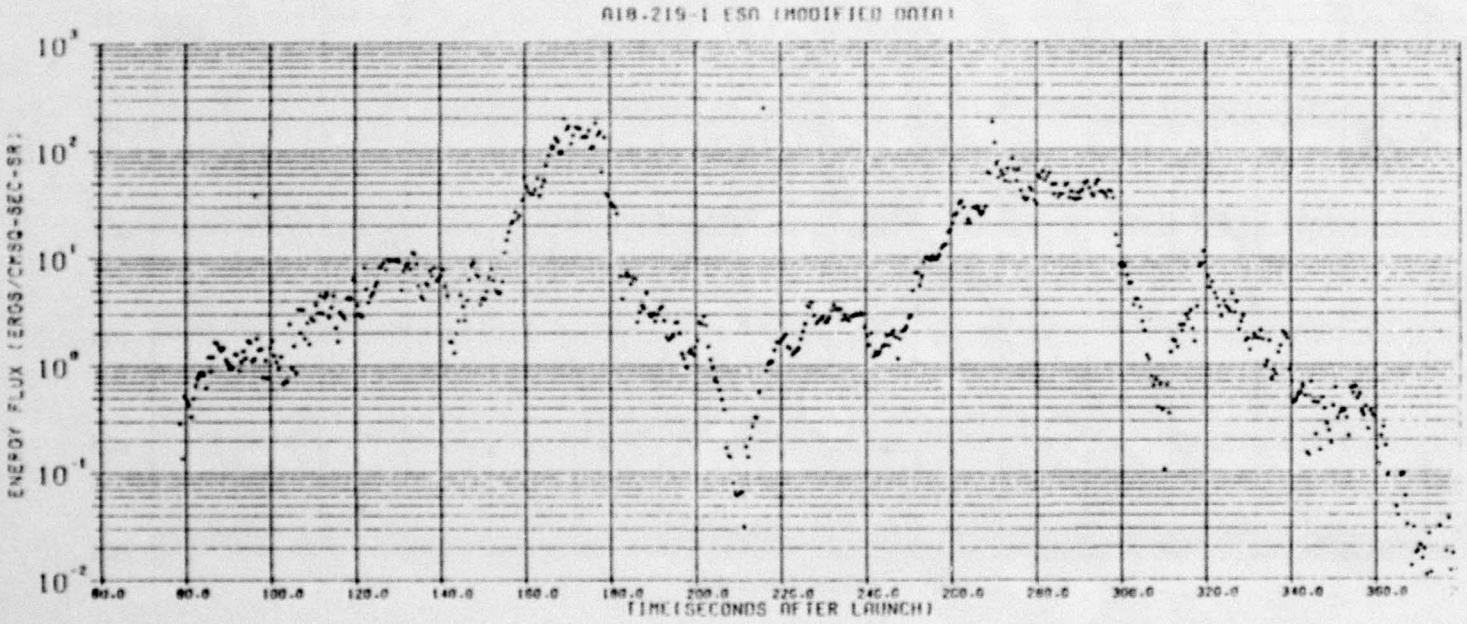

Figure 20. Energy flux that should be measured by the scintillator as calculated from the measured energy spectra.

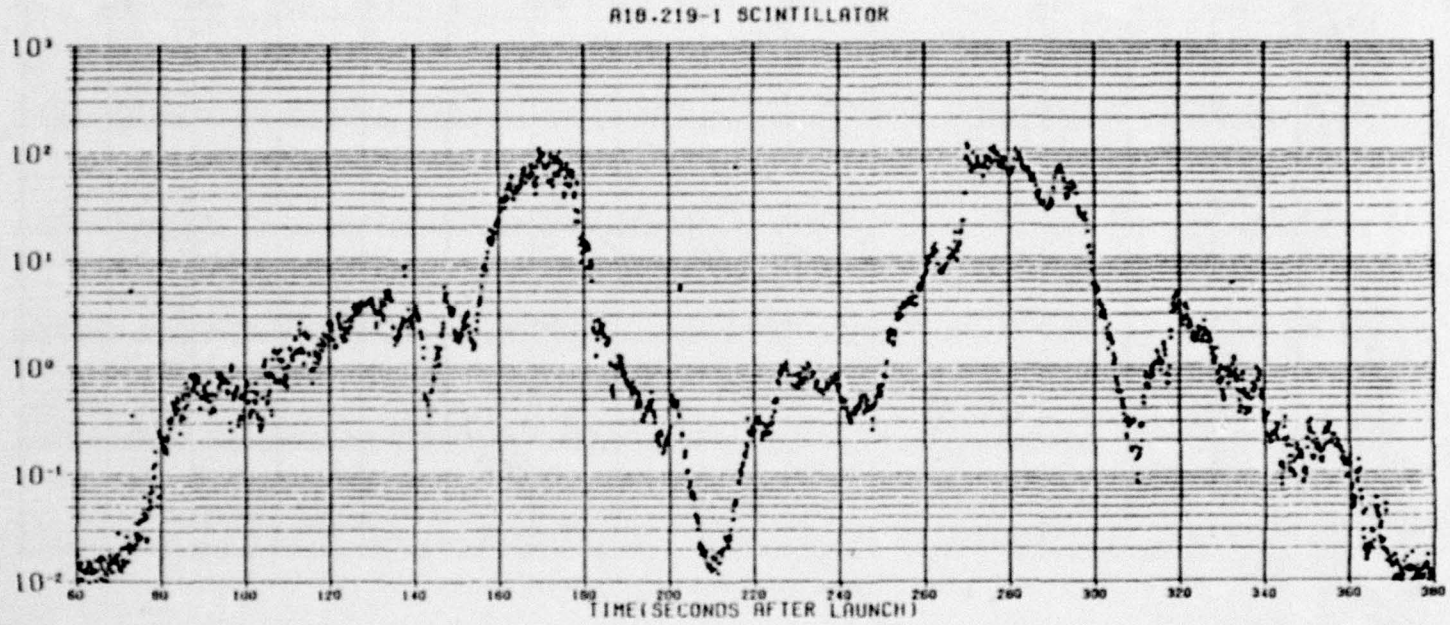

Figure 21. Energy flux measured by the scintillator on Rocket A18.219-1.

The total flux calculated from the measured ESA spectra is shown in Figure 22. Since part of the total flux was not measured by the ESA near the center of the arc, the peak flux of the auroral arc is greater than the measured peak flux of about 10^{10} electrons/cm^2-sec-sr. The structure of the total energy and total flux plots are very similar except that in a region where the energy flux is changing, the ratio of the energy fluxes is greater than the corresponding changes in the number fluxes, i.e., a change in energy flux corresponds to a change in the energy distribution of the electrons as well as a change in the total number of electrons. In addition it should be noted that the energy per unit flux is about a factor of two higher south of the arc and in the center of the arc than it is north of the arc, which indicates a softer spectrum north of the arc than in the arc or south of it.

5.2.2 Pitch Angle Distribution

The range of pitch angles covered by the ESA extended from about 35° to 55° and the range covered by the scintillator was from 45° to 55°. The rocket attitude control system maintained this range throughout the flight (during the period of the measurements). Since the electron flux was not measured at different pitch angles simultaneously, only those regions of the flight where the total flux remained essentially constant for a spin period could be used to study the pitch angle distribution. In the regions for which this condition was satisfied the data show that the pitch angle distribution was isotropic over the range from about 35° to 65°. A sample of the scintillator pitch angle distribution data at 175 seconds and 128 seconds is shown in Figure 23. The data indicate an isotropic pitch angle distribution within the spatial and/or temporal fluctuations occurring during the period of the measurement.

5.3 Ion-electric Production Rate and Electron Density Calculations

The production rate has been calculated with the assumption of an isotropic pitch angle distribution as is shown at two times during the flight in Figure 24. The production rates were based on measurements of the spectra made at 95 seconds (120 km) and 170 secs (183 km). In the latter case the peak intensity was not measured due to saturation of the instrument and the

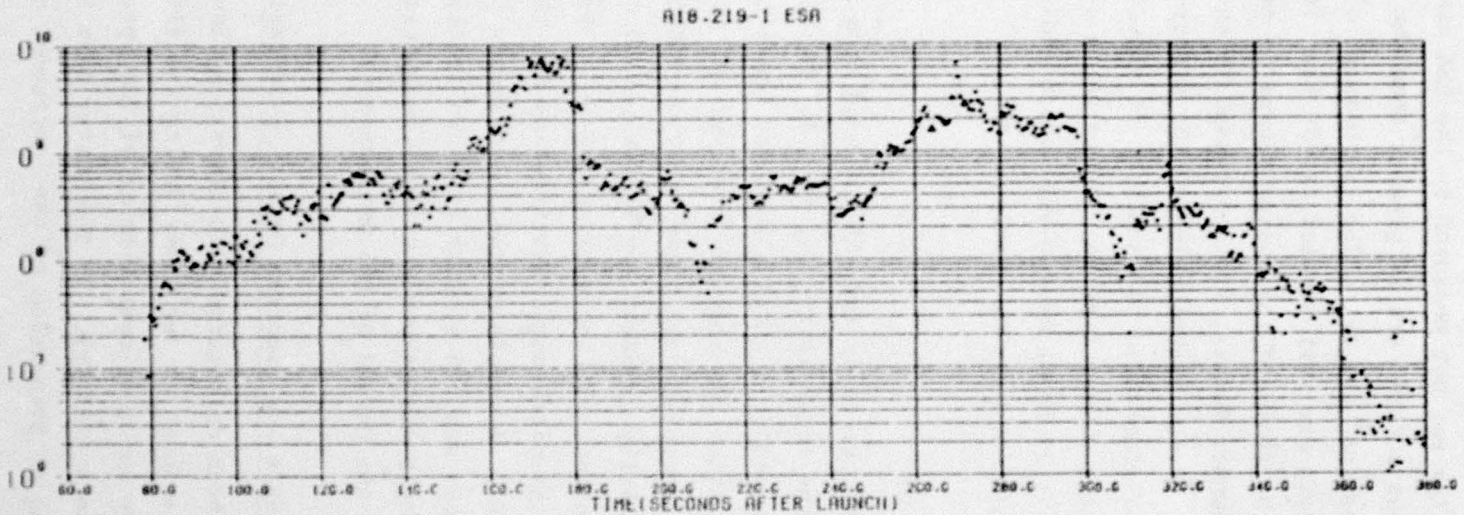

Figure 22. Electron flux calculated from the measured electron spectra for Rocket A18.219-1.

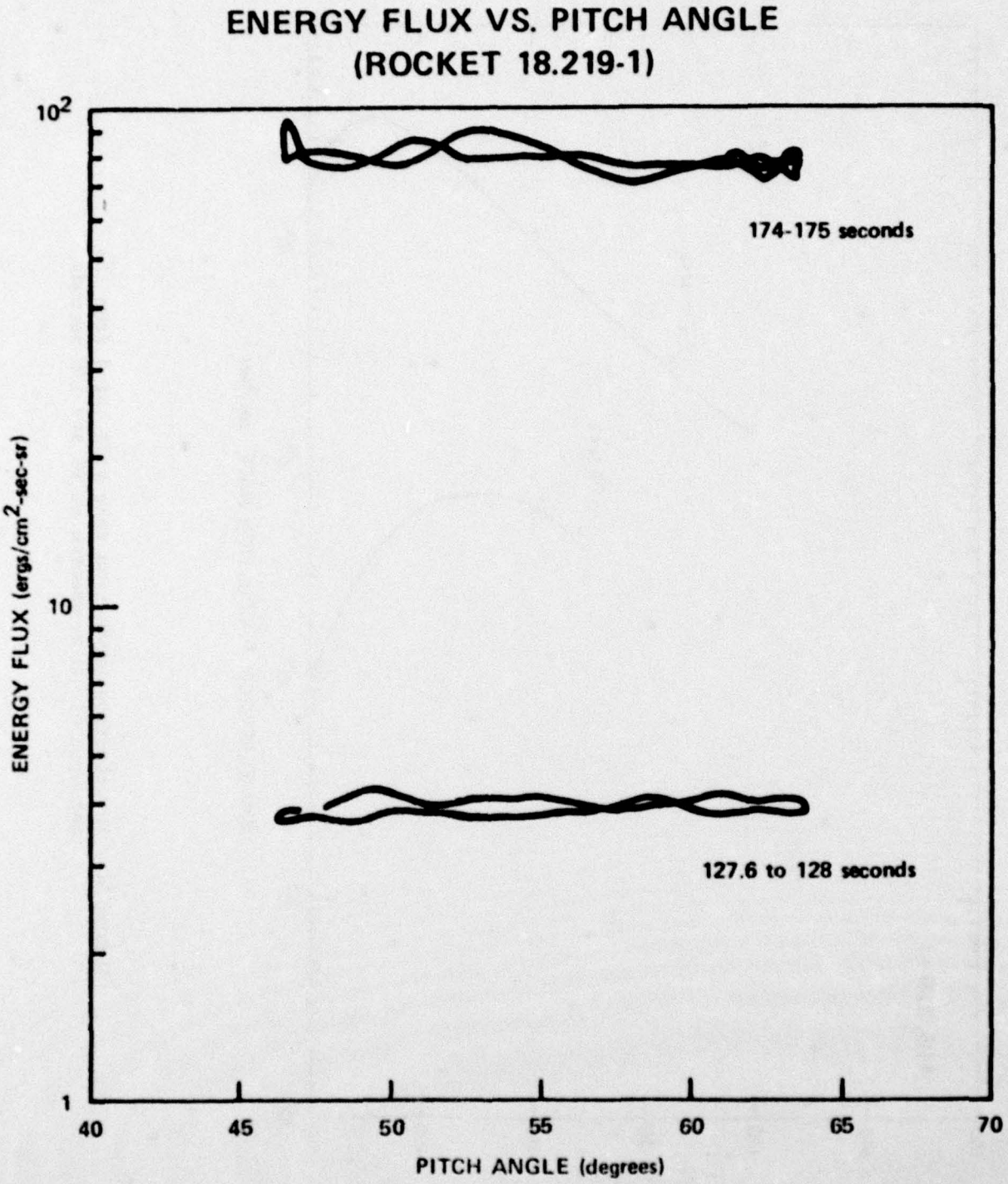

Figure 23. Pitch angle distribution measured by the scintillator at 174 and 128 seconds.

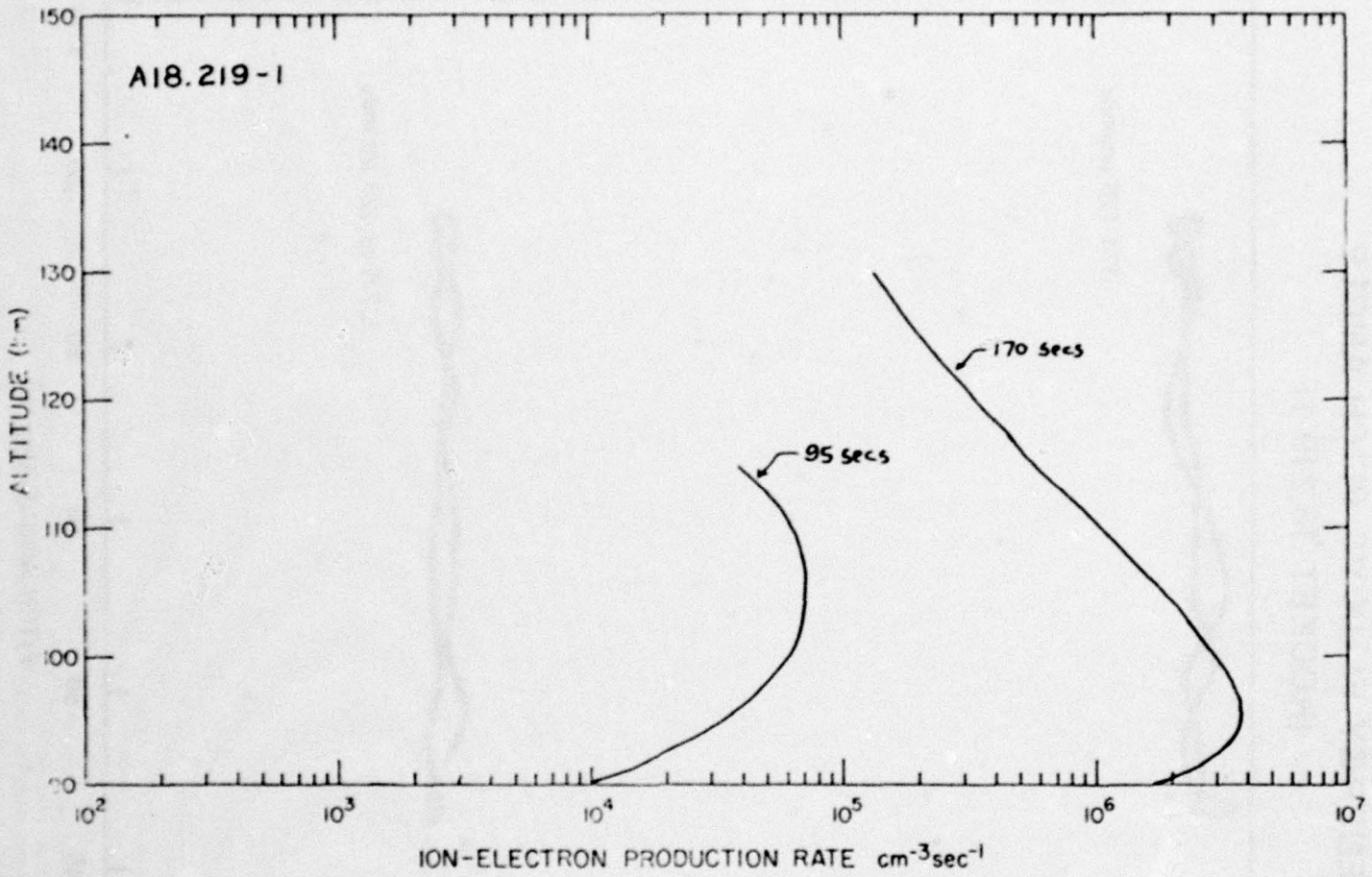

Figure 24. Ion-electron production rate calculated from the measured electron spectra at 95 and 170 seconds.

differential intensity was assumed to be equal to the saturated value in order to calculate the production rate. The total energy measured by the scintillator is consistently a factor of 2 to 3 lower than that calculated from the spectra measured by the ESA in regions where a complete spectrum is measured.

Since the scintillator was almost an order of magnitude lower than the energy flux measured by the ESA for rocket flight 18.205-1, whereas the ion density and 3914Å radiation calculated from the ESA spectra differed by less than a factor of two from their measured values it appears that there is a problem with the absolute calibration of the scintillator.

At 170 seconds the energy flux calculated from the ESA spectra is about twice that measured by the scintillator, which indicates that differential intensity of the spectra at saturation was not greatly different from its saturated value. This implies that the calculated production rate at 170 seconds should be within a factor of two of the actual production rate.

From the ion-electron production rate one can compute the electron density using $N_e = g/2$ where g is the production rate, N_e the electron density and α is the effective recombination coefficient [$\alpha = 3 \times 10^{-7} \left(\frac{300}{T}\right)$ and T is the temperature in °K][26]. The result is plotted in Figure 25 along with the positive density measured by the retarding potential analyzer from 90 to 120 km. The excellent agreement between the two curves indicates that the incident electron spectra are not changing appreciably from about 75 to 95 seconds. and that the calibration of the two instruments is within their expected accuracy.

---

[25] Swider, W., J. Atmos. Terr. Phys., 34, 1615 (1972).

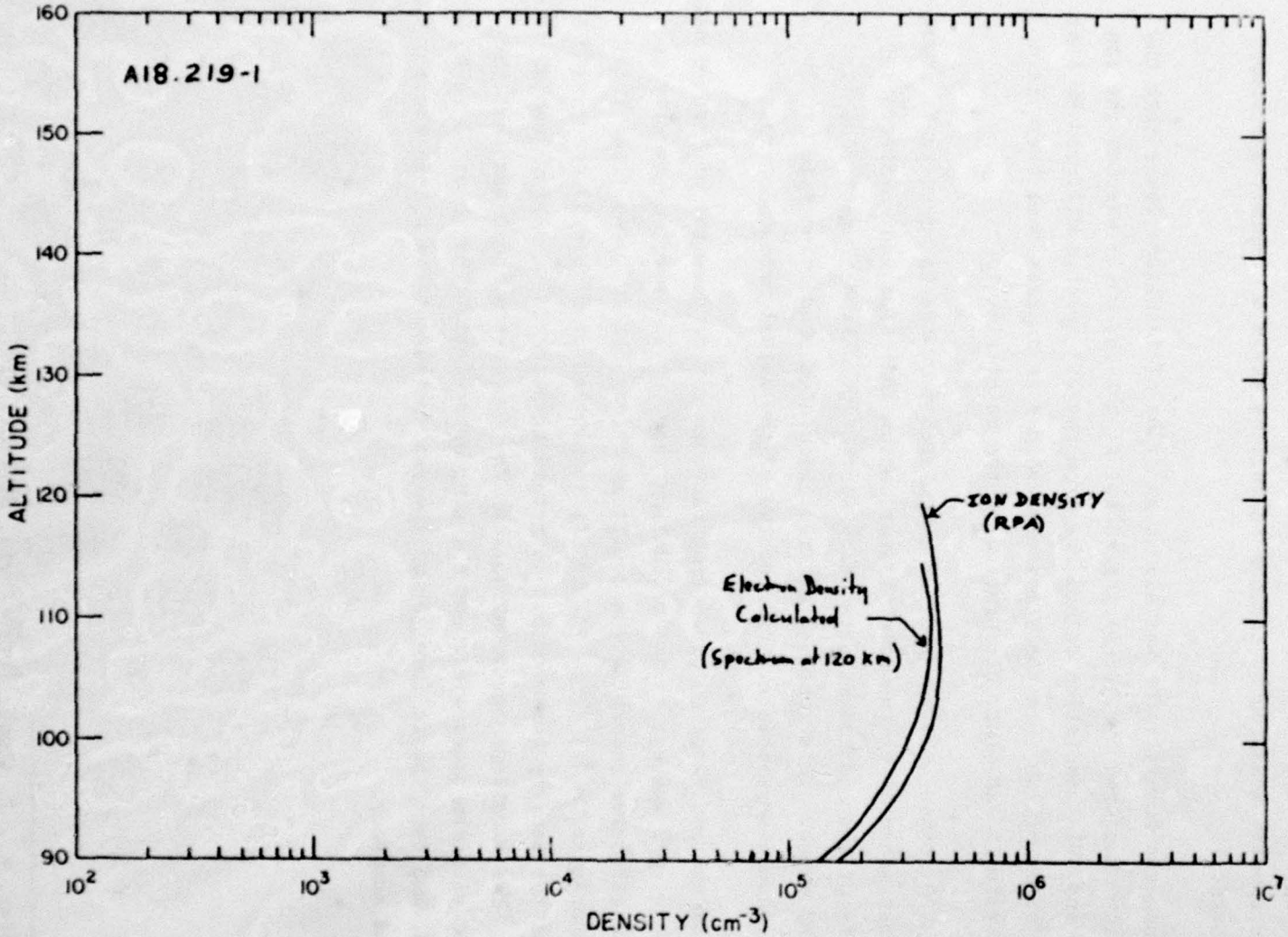

Figure 25. Positive ion density measured by the RPA compared with the density calculated from the production rate.

DISTRIBUTION LIST

DEPARTMENT OF DEFENSE

Director
Defense Advanced Rsch. Proj. Agency
Attn: LTC W.A. Whitaker

Defense Documentation Center
Attn: TC (2 Copies)

Director
Defense Nuclear Agency
Attn: TITL Tech. Library (3 Copies)
Attn: TISI Archives
Attn: RAAE Harold C. Fitz, Jr.
Attn: RAAE Lt. Col. William McKechnie
Attn: RAAE Capt. Peter Lund
Attn: RAAE Dr. Patrick Crowley

Dir. of Defense Rsch & Engineering
Department of Defense
Attn: DD/S&SS(OS) Daniel Brockway

Commander
Field Command
Defense Nuclear Agency
Attn: FCPR

Chief Livermore Division
FLD Command DNA
Attn: FCPRL

DEPARTMENT OF THE ARMY

Commander/Director
Atmospheric Sciences Laboratory
U.S. Army Electronics Command
Attn: DRSEL-BL-SY,A.F. Niles
Attn: H. Ballard

Commander
Harry Diamond Laboratories
Attn: DRXDO-NP, F.H. Wiminetz (2 Copies)

Director
BMD Advanced Technical Center
Attn: ATC-T, M. Capps
Attn: ATC-O, W. Davies

Dep. Chief of Staff for Rsch, Dev & Acout.
Department of the Army
Attn: MCB Division
Attn: DAMA-CSZ-C
Attn: DAMA-WSZC

Director
U.S. Army Ballistic Rsch Labs.
Attn: John Mester
Attn: Tech. Library

Commander
U.S. Army Electronics Command
Attn: Inst. for Expl. Research
Attn: Weapons Effects Section

Commander
CORADCOM
Attn: PP-Library
Attn: DRDCO-COM-D

DEPARTMENT OF THE NAVY

Commander
Naval Oceans Systems Center
Attn: Code 2200 William Moler

Director
Naval Research Laboratory
Attn: Code 7712 D.P. McNut
Attn: Code 6701 J.D. Brown
Attn: Code 2600 Tech Library
Attn: Code 7175J C.Y. Johnson
Attn: Code 6700 T. P. Coffey
Attn: Code 7709 Wahab Ali
Attn: Code 6780 D.F. Strobel
Attn: Code 6780 P. Juluenne
Attn: Code 6780 J. Fedder
Attn: Code 6780 S. Ossakow
Attn: Code 6707 J. Davis

Commander
Naval Surface Weapons Center
Attn: Code WA 501 Navy NUC Prgms. Off.
Attn: Technical Library

Superintendent
Naval Post Graduate School
Attn: Rsch Rpts Librarian

Commander
Naval Intelligence Support Ctr.
Attn: Document Control

DEPARTMENT OF THE AIR FORCE

AF Geophysics Laboratory, AFSC
Attn: LKB, K.S.W. Champion
Attn: OPR, A. T. Stair, Jr.
Attn: OPR, P.G. Doyle
Attn: OPR, R. Murphy
Attn: LKO, R. Huffman
Attn: OPR, J. Kennealy

AF Weapons Laboratory, AFSC
Attn: Maj. Gary Ganong, DES

Commander
ASD
Attn: ASD-YH-EX-LTC, R. Leverette

SAMSO/AW
Attn: SZJ Lt. Col. Doan

SAMSO/YN
Attn: Maj. P. Sivgals

AFTAC
Attn: Tech Library
Attn: TD

HQ
Air Force Systems Command
Attn: DLS
Attn: Tech Library
Attn: DLCAE
Attn: DLTW
Attn: DLXP
Attn: SDR
Attn: RDQ

US ENERGY RSCH. and DEV. ADMIN.

Division of Military Application
U.S. Energy Rsch & Dev Admin
Attn: Doc. Con.

Los Alamos Scientific Laboratory
Attn: DOC CON for H.V. Argo
Attn: DOC CON for M.B. Pongratz
Attn: DOC CON for R. Brownlee
Attn: Group AP-4, MA 567
Attn: DOC CON for J. Zinn

University of California
Los Alamos Scientific Laboratory
Attn: Librarian MS 362

Sandia Laboratories
Attn: DOC CON for W.B. Brown, Org. 1353
Attn: Tech. Library, Org. 3141

Argonne National Laboratory
Records Control
Attn: Doc. Con. for D.W. Green
Attn: Doc. Con. for LIR SVCS Rpts Sec
Attn: Doc. Con. for G.T. Reedy

University of California
Lawrence Livermore Laboratory
Attn: W.H. Duewer, L-262
Attn: J. Chang, L-71

U.S. Energy Rsch & Dev. Admin
Division of Headquarters Services,
Library Branch
Attn: Doc. Con. for Class. Tech. Lib.

OTHER GOVERNMENT

Department of Transportation
Office of the Secretary
Attn: S.C. Coroniti

NASA
Goddard Space Flight Center
Attn: Code 6801 A. Temkin
Attn: Tech. Library
Attn: Code 900 J. Siry

NASA
Langley Station
Attn: Tech. Library

NASA
Ames Research Center
Attn: N-245-3 R. Whitten

Department of the Army
Bal. Miss. Def. Adv. Tech. Ctr.
Attn: W.O. Davies

Federal Aviation Administration
Attn: HAPP/AEQ-10/James W. Rogers

Central Intelligence Agency
Attn: ED/SI RM 5G48 HG Bldg.
Attn: NED/OS I-2G4R HQS

Department of Commerce
National Bureau of Standards
Attn: Sec. Officer for M. Krauss
Attn: Sec. Officer for L.H. Gevantman

National Oceanic & Atmospheric Admin.
Environmental Research Laboratories
Department of Commerce
Attn: G. Reid
Attn: E. Ferguson
Attn: F. Fehsenfeld

DEPARTMENT OF DEFENSE CONTRACTORS

Science Applications, Inc.
Attn: D. G. Hopper

Aero-Chem Research Laboratories, Inc.
Attn: A. Fontijn
Attn: H. Pergament

Aerodyne Research, Inc.
Attn: F. Bien
Attn: M. Camac

Aerospace Corporation
Attn: N. Cohen
Attn: H. Mayer
Attn: R.J. McNeal
Attn: T.D. Taylor
Attn: J. Reinheimer
Attn: R.D. Rawcliffe
Attn: R. Herm

AVCO-Everett Research Laboratory, Inc.
Attn: Tech. Library
Attn: C.W. Von Rosenberg, Jr.

Battelle Memorial Institute
Attn: H.L. LaMuth
Attn: STOIAC

Brown Engineering Company, Inc.
Attn: N. Passino

General Research Corporation
Attn: D. Jones
Attn: J. Ise, Jr.

California at Riverside, University of
Attn: J.N. Pitts, Jr.

California at San Diego, University of
Attn: S. C. Lin

California University of Berkeley
Attn: Sec. Officer for H. Johnston
Attn: Sec. Officer for Dept of
Chem., H. L. Strauss

Calspan Corporation
Attn: C.E. Treanor
Attn: J.M. Grace
Attn: M.G. Dunn
Attn: W. Wurster

University of Colorado
Astro-Geophysics
Attn: J.B. Pearce

Colorado, University of
Office of Contracts and Grants
Attn: G.M. Lawrence, LASP

Concord Sciences
Attn: E.A. Sutton

University of Denver
Space Sciences Laboratory
Attn: B. Van Zyl

University of Denver
Denver Research Laboratory
Attn: Sec. Officer for D. Murcray

General Electric Company
Tempo-Center for Advanced Studies
Attn: DASAIC
Attn: W.S. Knapp
Attn: T. Stephens
Attn: D. Chandler
Attn: V.R. Strull

General Electric Company
Space Division
Attn: M.H. Bortner, Space Sciences Lab.
Attn: J. Burns
Attn: F. Alyea
Attn: P. Zavitsands
Attn: R.H. Edsall
Attn: T. Baurer

Geophysical Institute
University of Alaska
Attn: J.S. Wagner
Attn: N. Brown

Lowell University of
Center for Atmospheric Research
Attn: G.T. Best

Lockheed Missiles and Space Company
Attn: J. Kumer, Dept. 52-54
Attn: J.B. Cladis, Dept. 52-12, B202
Attn: B.M. McCormac, Dept. 52-54
Attn: T. James, Dept. 53-54
Attn: M. Walt, Dept. 52-10
Attn: R.D. Sears, Dept. 52-54

Institute for Defense Analysis
Attn: E. Bauer
Attn: H. Wolfhard

Mission Research Corporation
Attn: D. Archer
Attn: D. Fischer
Attn: M. Scheibe
Attn: D. Sappenfield
Attn: D. Sowle

Photometrics, Inc.
Attn: I.L. Kofsky

Berkeley Research Associates
Attn: J.B. Workman

Physical Dynamics, Inc.
Attn: A. Thompson

Physical Sciences, Inc.
Attn: K. Wray
Attn: R.L. Taylor
Attn: G. Caledonia

Physics International Compnay
Attn: Doc Con for Tech Library

Pittsburgh, University of the Comwlth
System of Higher Education
Attn: W.L. Fite
Attn: M.A. Biondi
Attn: F. Kaufman

R & D Associates
Attn: R. Latter
Attn: R.G. Lindgren
Attn: B. Gabbard
Attn: R. Lelevier
Attn: A.L. Latter
Attn: F. Gilmore
Attn: H.J. Mitchell

Rand Corporation
Attn: C. Crain

Science Application, Inc.
Attn: D.A. Hamlin
Attn: D. Sachs
Attn: D.G. Hopper

Stanford Research Institute International
Attn: M. Baron
Attn: W.G. Chesnut

Technology International Corporation
Attn: W.P. Boquist

United Technologies Corporation
Attn: H. Michels
Attn: R.H. Bullis

Utah State University
Attn: D. Baker
Attn: K. Baker
Attn: C. Wyatt
Attn: A. Steed

Visidyne, Inc.
Attn: H. Smith
Attn: J.W. Carpenter
Attn: T.C. Degges
Attn: C. Humphrey

Wayne State University
Attn: R.H. Kummler
Attn: W.E. Kaupplia

Commander
Rome Air Development Center
Attn: OSCA, J.J. Simons

Stewart Radiance Laboratory
Attn: R. Huppi

Boston College
Space Data Analysis Laboratory
Attn: E.R. Hegblom
Attn: W.F. Grieder

Forrestial Campus Library
Princeton University
Attn: Librarian